MODELING OF ELECTRONIC TRANSPORT IN NANOSTRUCTURES

Paula Havu

Laboratory of Physics
Helsinki University of Technology
Espoo, Finland

Dissertation for the degree of Doctor of Science in Technology to be presented with due permission of the Department of Engineering Physics and Mathematics, Helsinki University of Technology for public examination and debate in Auditorium K at Helsinki University of Technology (Espoo, Finland) on the 28th of October, 2005, at 13 o'clock noon.

Dissertations of Laboratory of Physics, Helsinki University of Technology
ISSN 1455-1802

Dissertation 135 (2005):
Paula Havu: Modeling of electronic transport in nanostructures
ISBN 951-22-7858-8 (print)
ISBN 951-22-7859-6 (electronic)

OTAMEDIA OY
ESPOO 2005

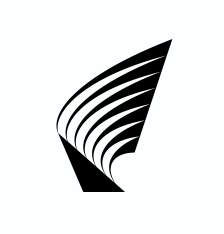

HELSINKI UNIVERSITY OF TECHNOLOGY P.O. BOX 1000, FI-02015 TKK http://www.tkk.fi	ABSTRACT OF DOCTORAL DISSERTATION

Author Paula Havu

Name of the dissertation

Modeling of electronic transport in nanostructures

Date of manuscript 9.9.2005	Date of the dissertation 28.10.2005

☐ Monograph ☑ Article dissertation (summary + original articles)

Department	Engineering Physics and Mathematics
Laboratory	Laboratory of Physics
Field of research	Computational physics
Opponent(s)	prof. Colin J Lambert
Supervisor	prof. Risto Nieminen
(Instructor)	prof. Martti Puska

Abstract

Nanometer-scale electronic devices are building blocks of future electronics. The function of these components is based on quantum-mechanical phenomena and therefore new modeling methods has to be developed to model properties of nano-devices. In this thesis one solution and implementation is presented.

In this thesis transport properties of the nano-devices are modeled using the density-functional theory. In the main part of the work electron densities and currents calculated using the Green's function method. The method enables the connection of the nanostructure to the semi-infinite leads by the open boundary conditions making finite-size effects small. Electron currents under finite bias conditions can also be calculated.

The use of the Green's function method is computationally heavy in comparison to the explicit wave-function methods. An important part of this thesis work is to choose efficient numerical methods and their implementation. The computer code created has one-, two- and three-dimensional versions so that different types of nanostructures can be modeled. The one- and two-dimensional versions use the effective mass approximation while the three-dimensional one uses nonlocal pseudopotential operators. The numerical implementation is done using the finite-element method with the so-called hp-elements.

The codes implemented are used to model magnetic resonance tunneling diodes, two-dimensional quantum wires, Na-atom chains and thin HfO2 layers.

Keywords nanostructure, electron transport, density-functional theory, finite-element method

Number of pages 112	ISBN (printed) 951-22-7858-8
ISBN (pdf) 952-22-7859-6	ISBN (others)
ISSN (printed) 1455-1802	ISSN (pdf)

Publisher Laboratory of Physics, Helsinki University of Technology

Print distribution

☑ The dissertation can be read at http://lib.tkk.fi/Diss/

Preface

This thesis has been prepared in the Laboratory of Physics at the Helsinki University of Technology during years 2001-2005. I have been working in the Computational Condensed-Matter and Complex Materials group (COMP).

I am grateful for Academy Professor Risto Nieminen for suggesting this research topic to me, providing facilities and conditions for the research, and also participating to the supervision work. I am indebted to Professor Martti Puska for excellent guidance and supervision during the research work and preparation of the papers. I wish to thank Dr. Ville Havu for his contribution to the work and help with the numerical methods. I also like to thank the members of the Electric Properties of Materials group for pleasant research atmosphere. I especially wish to thank Dr. Tuomas Torsti, M.Sc. Riikka Väänänen, M.Sc Noora Tuomisto, Dr. Adam Foster, M.Sc Mikko Hakala, Dr Harri Hakula, and Dr. Per Hyldgaard for contributing to this work.

Finally I would like to thank Ville for all the support and encouragement I got during this thesis work.

The financial support from the Väisälä foundation of the Finnish Academy of Science and Letters is gratefully acknowledged.

Helsinki, September 2005

Paula Havu

List of Publications

I P. Havu, T. Torsti, M. J. Puska, and R. M. Nieminen,
Conductance oscillations in metallic nanocontacts,
Phys. Rev. B **66**, 075401 (2002) (5 pages).

II P. Havu, V. Havu, M. J. Puska, and R. M. Nieminen,
Non-equilibrium electron transport in two-dimensional nano-structures modeled by Green's functions and the finite-element-method,
Phys. Rev. B **69**, 115325 (2004) (13 pages).

III P. Havu, M. J. Puska, R. M. Nieminen, and V. Havu,
Electron transport through quantum wires and point contacts,
Phys. Rev. B **70**, 233308 (2004) (4 pages).

IV P. Havu, N. Tuomisto, R. Väänänen, M. J. Puska, and R. M. Nieminen,
Spin dependent electron transport through a magnetic, resonant tunneling diode
Phys. Rev. B, **71**, 235301 (2005) (12 pages).

V P. Havu, V. Havu, M. J. Puska, M. H. Hakala, A. Foster,
and R. M. Nieminen,
Finite-element implementation for electron transport in nanostructures,
submitted to Jour. of Chem. Phys. (9 pages).

The author has had an active role in all stages of the research work reported in this thesis. She has been the main responsible person for developing and implementing the one-, two- and three-dimensional Green's function codes reported in Publications **II**-**V**. MSc Riikka Väänänen has participated in the implementation of the one-dimensional Green's function solver of Publication IV. The author has had the main responsibility for the calculations reported in Publication **I**-**III** and **V**, and in the part of the Publication **IV** which includes the calculations using the Green's function method. She has contributed actively to the planning, the calculations and the writing of all the Publications.

Contents

Chapter 1

Introduction

Rapid development of electronic circuits has produced new and fast devices, for example computers with high calculation capacity. This has had a big effect in computational science so that, for example, the calculations of this thesis have become possible. The major trend of the development of electronic components is to improve fabrication methods so that the size of the components becomes smaller and more circuits can be included on a chip. Smaller components also work with smaller currents and voltages and therefore more efficiently with less energy consumption. However, the diminishing of the size cannot go on forever. In the nanometer-scale devices the electron wavelength on the Fermi-level is comparable to the feature size and quantum mechanical effects arise. On the other hand, these effects are not necessarily harmful, as they can also be used to design totally new types of electronic components. Nano-electronic components can produce same functions as traditional components, for example amplification or logic-gate operations. The physics behind their function is, however, different. Besides the possible use in nano-electronic components, nanostructures also offer a platform to explore the fundamental physics of interacting electrons.

Different layer structures and single atoms or molecules between two electrodes are typical nanostructures. Various types of nano-devices have recently been objects of intensive research. Fabrication and measuring techniques have developed so that the results are of good quality with low noise and systematic behavior between samples. At the same time the theoretical interest in explaining the properties of these structures has increased as well. Many theoretical methods used previously in modeling bulk materials properties have been transferred to model the new structures. However, some nanostructures have characteristic properties that pose problems when old methods are applied directly. One of them is that nanostructures, in contrast to crystal lattices, do not have repeating structures which would enable the use of the periodic boundary conditions. If the periodic

boundary conditions are used anyway, spurious finite-size effects can appear.

In this work we have modeled electronic structures and transport properties of nanostructures. In the main part of the work the Green's function method is used combined with the density-functional theory (DFT). Using the Green's function method a system can be made effectively infinite with only small remaining finite-size effects. It is also possible to calculate the electric current through the nanostructure when there is a finite bias voltage over the system. The downside of the Green's function method is that it is computationally heavy as compared to the wave-function methods available for periodic systems.

During this work the Green's function-DFT scheme was implemented as computer programs using the finite-element method. There are three different programs, namely one-, two- and three-dimensional versions, in order to model different types of nanostructures. Because the development of the methods and implementing the solvers was quite a large part of the work, they occupy a relatively large part of this summary.

The results of the work are published in articles **I**-**V**. In Publication **I** the modeling is done using the MIKA code [1]. There the real-space wave-function method is used and conductances of sodium atom chains are calculated using the Friedel sum rule. These results are compared later with the Green's function calculations. In the other Publications **II-V** the Green's function method is used. Publication **IV** uses the mathematically one-dimensional version, Publications **II** and **III** the two-dimensional version and Publication **V** the three-dimensional version. In every paper the theoretical and numerical schemes to solve these systems are explained.

The organization of this thesis summary is as follows. In Chapter 2 the general transport properties of nanostructures are introduced. In Chapters 3 and 4 the theoretical background and the numerical methods are explained, respectively. Chapter 5 is a summary for the results of the modeled nanostructures.

Chapter 2

Nanostructures between electrodes

In nanostructures physical phenomena depend on features with dimensions of the order of nanometers. Examples of nanostructures include thin atomic layers, single molecules, atomic clusters and chains and structures such as quantum dots and wires manufactured in to the two-dimensional electron gas at semiconductor interfaces. The fabrication and the modeling methods of these various nanostructures are quite different. In this chapter an introduction to these aspects is given. More specifically, in this thesis transport properties of nanostructures are modeled. We concentrate on the nano-scale systems connected to leads used to measure the current as a function of the bias voltage. The fabrication and modeling of isolated nanostructures are different subjects and not considered here.

2.1 Fabrication and measuring techniques

Most of the current fabrication and measurements of nano-scale devices concentrate on single components, not on complicated circuits. A typical problem is that even if properties are qualitatively similar, differences appear easily between different samples. For small nano-devices which consist of only few atoms or molecules the controlled fabrication is not easy. Even one impurity in a wrong place can have a huge impact on conductance. However, in many measurements the purpose is not to build an amplifier or an other functional device, but to investigate the basic physical properties, for example, the chemical bonds between atoms. This kind of measurements are done, for example, using a scanning tunneling microscope.

A scanning tunneling microscope has a sharp tip which is brought close to the substrate surface [2]. The tip and the surface are made of conducting material,

so that a small bias voltage between them causes an electron tunneling current. It is possible to image the surface by sweeping the tip near the surface so that the tunneling current is kept constant by varying the height of the tip from the surface. The recorded height position of the tip gives the structure of the surface within the atomic resolution. Using this method it is also possible to measure the conductance of a single molecule. The molecule is located on the surface and the tip is placed on top of it. By changing the distance between the tip and the surface it is possible to control the connection between the tip and the molecule. An example is given Figure 2.1 where a benzene-1,4-dithiolate molecule is placed between two electrodes. In this molecular electronics the basic characteristics of devices are mainly determined by the chemical properties of the molecules involved.

An atomic chain can also be made using the scanning tunneling microscope. There the tip is brought in contact with the surface and then slowly drawn away so that a small atomic wire is formed in the contact region. Another option is atomic wires made by breaking the metallic connection by a piezoelectric sample holder (mechanically controlled break junction technique) [3].

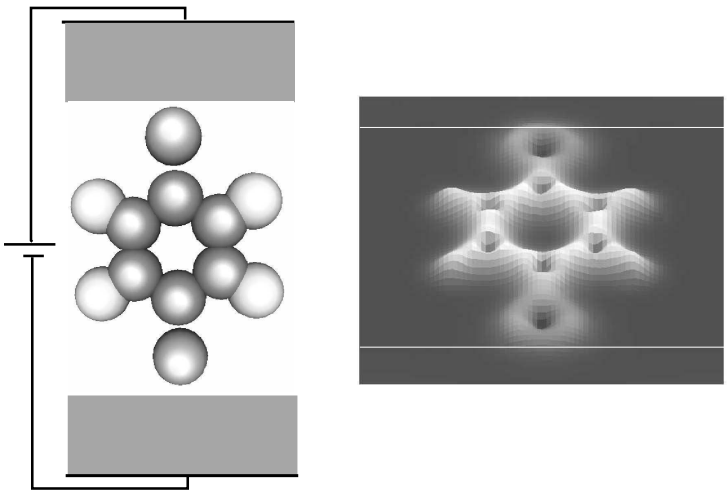

Figure 2.1: Example of a molecular electronic system, the benzene-1,4-dithiolate molecule placed between two electrodes. Left: the schematic picture of the biased system. Right: the calculated electron density on the plane intersecting the atoms.

There are nanostructures which consist of many atoms and the properties of which can be more artificially varied than those in the molecular electronics [4, 5, 6]. The idea of these devices is presented schematically in Figure 2.2. These devices are made, for example, using the semiconductor heterostructure techniques so that

two different semiconductors (for example, GaAs and GaAlAs) are evaporated on top of each others. The movement of electrons is strongly restricted in the interface between the semiconductors so that electrons form a two-dimensional electron gas.

Two-dimensional nanostructures have interesting properties. The impurities responsible the doping region are located far away from the interface, reducing electron scattering from impurities and increasing the mean free path. The Fermi wavelength is also large as compared to the dimensions of the nanostructure. In order to make different types of nanostructures, such as quantum dots, quantum wires and quantum antidots, the electron motion has to be restricted also in directions along the interface. This is done using metallic gates which are evaporated on the top of the layer structure. This makes it possible to vary the size and shape of the device in a controlled way.

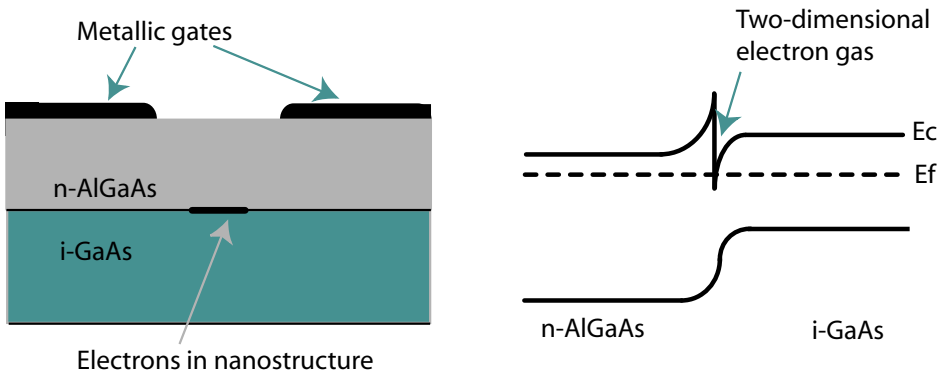

Figure 2.2: In two-dimensional nanostructures two-dimensional electron gas is located in the interface between AlGaAs-GaAs. Metallic gates are used to restrict the electrons so that nanostructures are formed. Left: schematic picture of two-dimensional nanostructures. Right: band diagrams at the AlGaAs-GaAs interface.

An other group of semiconductor nano-systems are the atomic layer structures. They are hetero-structures in which thin layers of different semiconductor materials are evaporated on the top of each others. Adjacent semiconductor layers have different band gaps forming potential barriers for electrons moving in the perpendicular direction. Distances between potential barriers are so small that electron states are quantized in the direction of the transport. One of the most common devices of this kind is the resonant tunneling diode, which has two potential barriers and between them a quantum well hosting resonance states for electrons. Other heterostructures are, for example, thin insulating oxide layers in CMOS transistors.

2.2 Electron transport through nanostructures

When electrons move in a material they scatter from impurities, other lattice defects and from phonons. Usually, the scattering from other electrons is less important [7]. The scattering causes electrical resistance. In normal-size electronic components this resistance follows Ohm's law for the current I and voltage V, so that the resistance R is proportional to the length L of the device

$$V = RI = \rho_R \frac{L}{A} I. \tag{2.1}$$

Above, ρ_R is the resistivity of the material and A the perpendicular area of the device. Ohm's law is understandable, because typically the scatterers are uniformly distributed into the material. A longer device has also more scatterers to destroy the collective electron drift movement. If we make the device smaller the number of scatterers diminishes. In this Thesis we consider very small devices where there are no impurity scatterers. In this regime it is not surprising that the statistical Ohm's law is not valid and other theories have to be used.

The electron transport properties of devices can be characterized by the de Broglie wavelength, the mean free path and the phase-relaxation length of electrons. Ohm's law is valid for devices which have dimensions much longer than these lengths. The de Broglie wavelength is here the electron wavelength at the Fermi-level. If the size of the device is of the same order of magnitude as the de Broglie wavelength, quantum mechanical phenomena appear. For example, electrons have a discrete energy spectrum. The mean free path of the electrons tells how long a distance an electron moves in average before it has lost its original momentum by scattering. Because in a typical collision an electron loses only a part of the momentum the mean free path is longer than distances between individual collisions.

The phase-relaxation length is the average length which an electron can move before collisions destroy its original phase. As in the case of the mean free path a single collision destroys only a part of the phase. More specifically, in order to affect the electron phase, collisions have to be inelastic, so that typically the phase-relaxation length is longer than the mean-free path. If the size of the device is smaller than the phase-relaxation length, waves of electrons interfere and quantum mechanical phenomena appear. These phenomena have large effects on the transport properties of devices. This is the case in a typical nanostructure at least as a first approximation. In this work we concentrate only on the coherent transport of electrons and ignore the inelastic effects.

In two-dimensional nanostructures, which are introduced in Chapter 2.3, the phase-relaxation length is typically large and the de Broglie wavelength of an electron is comparable to the size of the device. Consider next a two-dimensional wire of

length L between two large electrodes or electron reservoirs. In the wire electron states in the perpendicular direction of the wire are quantized. The electron density per unit length corresponding to a given perpendicular state in the momentum range between k and $k + dk$ and spin σ is

$$n_\sigma(k)\,dk = \frac{1}{L}\frac{L}{2\pi} f_\sigma(k)\,dk = \frac{1}{2\pi} f_\sigma(k)\,dk, \tag{2.2}$$

where $f_\sigma(k)$ is the Fermi distribution function and k is the projection of the wave vector along the wire direction. Note that we use the SI units in this chapter for clarity and not the atomic units as in the remaining chapters of the thesis. For small bias voltages the electrodes are approximately in the equilibrium and have local quasi Fermi-levels with distribution functions $f_{R\sigma}(k)$ and $f_{L\sigma}(k)$ for the right and left lead, respectively. In contrasts the wire region does not have a well defined Fermi-level. The electron current carried by one perpendicular state, the so-called conducting mode, is

$$I = \sum_\sigma \int_0^\infty e\, v_\sigma(k)\, n_\sigma(k)\, dk = \sum_\sigma \int_0^\infty e\, \frac{\hbar k}{m_e^*} \left(\frac{f_{R\sigma}(k)}{2\pi} - \frac{f_{L\sigma}(k)}{2\pi} \right) dk. \tag{2.3}$$

Above $v(k)$ is the electron velocity along the wire and m_e^* is the electron effective mass. In the zero temperature limit the Fermi distributions are step functions so that Equation (2.3) has the form

$$I = \sum_\sigma \int_{\sqrt{2m_e\mu_L}/\hbar}^{\sqrt{2m_e\mu_R}/\hbar} e\, \frac{\hbar k}{m_e}\, \frac{1}{2\pi} dk = \sum_\sigma \frac{e^2}{h} \frac{\mu_R - \mu_L}{e} = \sum_\sigma \frac{e^2}{h} V_B, \tag{2.4}$$

where $\mu_{R/L}$ are the chemical potentials of the leads and their relative values depend on the bias voltage V_B so that $\mu_R - \mu_L = eV_B$. From Equation (2.4) we see that the conductance of one conducting mode, the so-called conductance quantum is

$$G_0 = \frac{2e^2}{h}. \tag{2.5}$$

It is the maximum conductance of a single conducting mode with two spin states. In practice, a mode is not necessarily fully conducting, because electrons can scatter in the nanodevice and at its connections to the electrodes. The probability for an electron to pass the device in the conducting mode i is marked by $T_{i,\sigma}$. Now the total conductance of the wire has the form

$$G = \sum_{\sigma,i} \frac{e^2}{h}\, T_{\sigma i}. \tag{2.6}$$

This equation is the so-called Landauer formula for the conductance [8]. It tells that the conductance of a thin wire stays finite even for small values of the length

L. The conductance increases to infinity, meaning zero resistance, if we have a large device for which the number of conducting modes is infinite. However, a very large number of conducting modes means a large device which is no longer considered to be a nanodevice. The same result of Equation (2.6) can also be derived for three-dimensional systems. This kind of quantization of the electron conductance is seen in many systems, for example, in quantum wires and in atomic chains which we have modeled in this thesis (see Chapter 5). The Green's function method used in this thesis is analogous to this formula.

2.3 Models for nanostructures

Transport properties of nano-structures are modeled using different quantum-mechanical methods approximating different properties of the structure. In some simulations electron interactions are included carefully so that many-particle effects are included. These models include, for example, the Kondo model and the Anderson impurity model [9]. Nanostructures in these models do not have any specific geometry, they are just considered as discrete electron states.

Other groups of models consider the specific shape of the nanostructure. The discrete atomic structure can also be included. This means that it is possible to get information about the effects of structural changes of the system. Typically, the electron-electron interactions are then included in a mean-field manner. This means that some many-particle effects can not be seen.

In this work the density-functional theory (DFT) is used. It is a mean field theory which is successfully used in computational materials physics and chemistry obtaining results in good quantitative agreement with measurements. In order to model transport properties the nanostructure is connected to the electrodes. This means that the size of the system is infinite. In practice, we have to define the calculation volume Ω to be finite. In Publication **I** this is done simply by making the leads large but finite. This system is easy to implement and solve, but the bad consequence is that the finite-size effects are large. The other possibility is that periodic boundary conditions are employed, so that the size of the system is infinite. However, the system can still suffer from finite size effects, due the finite number of wave functions used in the modeling and the interaction of the system with its artificial periodic images.

In order to handle the finite-size effects we use the scattering formalism. The model is depicted in Figure 2.3. The system is divided into three regions: the calculation volume Ω, the left lead Ω_L and the right lead Ω_R. At the boundaries $\partial\Omega_{P1}$ and $\partial\Omega_{P2}$ the electron density vanishes or the periodic boundary conditions

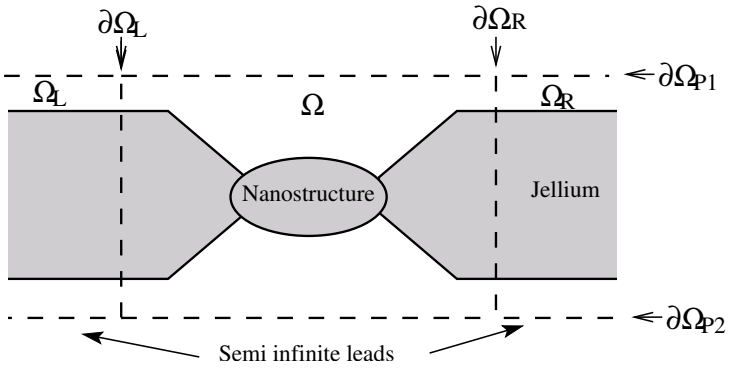

Figure 2.3: Schematic sketch about a nanostructure between two lead of infinite size.

are applied. Open boundary conditions are applied at the boundaries $\partial\Omega_L$ and $\partial\Omega_R$. The open boundary conditions mean that electrons can travel through the boundary without any reflection so that there is a continuous flow of electrons from the leads and at the same time other electrons are leaving the central calculation volume Ω through the boundaries $\partial\Omega_L$ and $\partial\Omega_R$.

The electron density and the current for an open scattering system can be modeled in different ways. One possibility is to solve the electron wave functions in the central region for the open system. The wave functions obey the open boundary conditions which depend on electron energy, so that there exist an infinite number of wave functions. This is because for an infinite system the energy spectrum of electrons is continuous. Because the central quantity is the total electron density, calculations include integrations over the electron energy so that only a finite number of wave functions are actually calculated. Typically energy integration paths include rapid variations, for example sharp resonance peaks, so that a large amount of wave functions are needed making the calculations heavy.

The scattering problem can also be formulated using the Green's function approach. In the continuum limit this gives the same results as the scattering wave function method. We have used the Green's function method in the major part of the present work (Publications **II**-**V**). In the Green's function method many-body interactions can be in principle fully included [10]. However, in practice, the calculations are computationally so heavy that the use of the DFT is justified. There are also many other implementations using the DFT and the Green's function method [11, 12, 13, 14, 15, 16, 17, 18, 19, 20, 21, 22].

2.3.1 Units

In all other chapters except Chapter 2.2, we use the atomic units or effective atomic units in the equations. In the atomistic calculations the atomic units are used. There the elementary charge $e = 1$, electron mass $m_e = 1$, dielectric constant $\epsilon = 1$, and the Planck constant $\hbar = 1$. The unit of distance is the Bohr radius (a_0), and the energy unit hartree (Ha).

The effective atomic units are used in the one- and two-dimensional models. They are related on the effective-mass approximation, in which an electron in a semiconductor lattice is modeled as a free electron with an effective mass. In the effective atomic units the effective electron mass and the dielectric constant are set equal to unity, i.e. $m^* = \epsilon^* = 1$. The effective atomic units are transformed to the usual atomic units and SI units using the relations

Length:	$1\,a_0^*$	$= 1\frac{\epsilon}{m^*}a_0$	= 0.529 $\frac{\epsilon}{m^*}$ Å
Energy:	$1\,\mathrm{Ha}^*$	$= 1\frac{m^*}{\epsilon^2}\mathrm{Ha}$	= 27.2 $\frac{m^*}{\epsilon^2}$ eV
Current:	$1\,\mathrm{a.u.}^*$	$= 1\frac{m^*}{\epsilon^2}\mathrm{a.u.}$	= 6.62 $\frac{m^*}{\epsilon^2}$ mA

Chapter 3

Theoretical basis

3.1 Density-functional theory

In the nanostructures, there are many electrons in a region where electron states are quantized in some directions. The stationary properties of the system are calculated from the many-particle Schrödinger's equation

$$\hat{H}_M \Psi(\mathbf{r}_1, ..., \mathbf{r}_N) = E\Psi(\mathbf{r}_1, ..., \mathbf{r}_N), \tag{3.1}$$

where E is the energy of the many-particle electron state and the many-particle Hamiltonian operator is defined as

$$\hat{H}_M = \sum_i \left(-\frac{1}{2m}\nabla_i^2 \right) + \sum_i V_{\text{ext}}(\mathbf{r}_i) + \frac{1}{2}\sum_{i \neq j} \frac{1}{\mathbf{r}_i - \mathbf{r}_j}. \tag{3.2}$$

Above, $\mathbf{r}_i$ are the coordinates of the electrons. Solving these equations is computationally heavy, because the total many-particle wave function Ψ depends on many variables. In our model it is impossible, because we have an infinite system with an infinite number of electrons. This is why it is more practical to take the electron density ρ as the basic variable. It is calculated from Ψ as

$$\rho(\mathbf{r}) = N \int d\mathbf{r}_2 ... \int d\mathbf{r}_N |\Psi(\mathbf{r}, \mathbf{r}_2, ..., \mathbf{r}_N)|^2. \tag{3.3}$$

According to the Hohenberg-Kohn theorem [23] all of the ground state properties can also be calculated from the electron density. Because the electron density depends only on one spatial variable, $\mathbf{r}$, the solution of the system is a more realistic task. In order to do that we use the variational principle

$$E = \langle \Psi | \hat{H}_M | \Psi \rangle \;\; \leq \;\; \langle \Psi' | \hat{H}_M | \Psi' \rangle, \tag{3.4}$$

where the particle number of the system is constant and Ψ' is a approximate solution of the wave function. This means that the correct Ψ minimizes the total energy. In the DFT the minimizing problem can be written in the form of the Kohn-Sham equations [24, 25, 26, 27]

$$\hat{H}\psi_i(\mathbf{r}) = \epsilon_i\,\psi_i(\mathbf{r}), \tag{3.5}$$

$$\hat{H} = -\frac{1}{2}\nabla_i^2 + V_{\text{ext}}(\mathbf{r}) + V_{\text{c}}(\mathbf{r}) + V_{\text{xc}}(\mathbf{r}), \tag{3.6}$$

$$\rho(\mathbf{r}) = \sum_{i=1}^{N} |\psi_i(\mathbf{r})|^2, \tag{3.7}$$

$$V_{\text{c}}(\mathbf{r}) = \int \frac{\rho(\mathbf{r}')}{|\mathbf{r}-\mathbf{r}'|} d\mathbf{r}', \tag{3.8}$$

$$V_{\text{xc}}(\mathbf{r}) = \frac{\delta E_{\text{xc}}[\rho(\mathbf{r})]}{\delta\rho(\mathbf{r})}. \tag{3.9}$$

Note that above $\hat{H}$ is the single-particle Hamiltonian operating on the single-particle wave functions. These single particle wave functions ψ_i and eigenenergies ϵ_i do not have any strict physical meaning. They are just auxiliary functions in order to calculate the electron density. The Kohn-Sham equations still include many-particle effects because the effective potential has the terms $V_{\text{c}} + V_{\text{xc}}$. The Hartree potential V_{c} includes the average Coulomb interactions caused by the electron density ρ. The exchange-correlation part V_{xc} includes the remaining parts of the electron-electron interactions. These equations give the correct electron density and the electron density gives the correct total energy of the system. However the computational task is much easier because we do not need to solve the many-particle wave function anymore.

In theory, the Kohn-Sham equations give the correct properties for the many particle system. In practice, we cannot solve for the exchange-correlation potential exactly, but some approximations have to be done. The most widely used approximation is the local density approximation (LDA), which we have also used in this work. It means that the exchange-correlation energy is expanded to a series as a function of the density gradients and cut after the first term, i.e. the result is

$$E_{\text{xc}}[\rho_\uparrow, \rho_\downarrow] = \int \rho(\mathbf{r})\epsilon_{\text{xc}}\left(\rho(\mathbf{r})\right) d\mathbf{r} \tag{3.10}$$

where $\epsilon_{\text{xc}}(\rho(\mathbf{r}))$ is the exchange-correlation energy per electron for the uniform electron gas with the density $\rho(\mathbf{r})$. LDA works for systems with slowly-varying electron densities. In many cases it works well even in systems where the electron

density varies remarkably (atoms, molecules, solids). If more accurate results are needed gradient correction methods can be applied. We have used in our solver dedicated for the two-dimensional electron gas systems $V_{\rm xc}$-potentials calculated and parameterized by Attaccalite *et. al* [28, 29]. In the three-dimensional cases we have used the parameterization by Perdew and Zunger [30, 31].

The DFT is derived for the ground-state equilibrium states. In this work we also consider non-equilibrium systems in which a finite bias voltage is applied between the leads. It is not clear how well the DFT describes these systems [32, 33]. It may be that better exchange-correlation potentials should be used. We assume in this work that the DFT within the LDA can still give a reasonable approximation for properties of the nanostructures also in non-equilibrium, current-carrying situation.

3.2 Green's function method

In Publications **II-V** we have combined the Green's function technique [4, 34] with the DFT. Instead of the single-particle wave functions, solved from (3.5), we use the single-particle Green's functions as the auxiliary functions in the Kohn-Sham equations. This is done in order to implement open boundary conditions, to add the finite bias-voltage between the leads and to calculate the current as explained in Chapter 2.3. Note that for clarity the equations are written for a spin-compensated system. The generalization to spin-polarized systems is straightforward.

The calculations start from the retarded Green's function G^r defined by

$$\big(\omega - \hat{H}(\mathbf{r})\big)G^r(\mathbf{r},\mathbf{r}';\omega) = \delta(\mathbf{r}-\mathbf{r}'), \tag{3.11}$$

where ω is the electron energy and $\hat{H}$ is the DFT Hamiltonian (3.6) of the system. Equation (3.11) gives also the advanced Green's function, G^a as the other solution. In practice, the separation of these two solution is done using boundary conditions. When we know G^r, the so-called lesser Green's function $G^<$ can be calculated. When there is no bias voltage, the system is in the equilibrium and $G^<$ is calculated as

$$G^<(\mathbf{r},\mathbf{r}';\omega) = 2f_{L/R}(\omega)\, G^r(\mathbf{r},\mathbf{r}';\omega). \tag{3.12}$$

Above, $f_{L/R}$ are the Fermi functions of the leads ($f_L = f_R$ in equilibrium). For a finite bias voltage a more complicated form has to be used. The system is divided into three parts Ω, Ω_L, and Ω_R as explained in the previous section in Figure 2.3. We then write (3.11) in the form

$$\big(\omega - \hat{H}_0 - \Sigma_L^r(\omega) - \Sigma_R^r(\omega)\big)G^r(\mathbf{r},\mathbf{r}';\omega) = \delta(\mathbf{r}-\mathbf{r}'), \tag{3.13}$$

where $\hat{H}_0$ is the Hamiltonian of the isolated region Ω and $\Sigma^r_{L/R}$ are the so-called self-energies of the leads. This name comes from an analogy with the many-body Green's function theories, where self-energies are calculated for different interactions, for example, the electron-electron or electron-phonon interactions. $\Sigma^r_{L/R}$ is the interaction term between the electrons in Ω and the electrons in $\Omega_{L/R}$. The derivation of these terms is presented in Publication **II**.

We also define the Γ-functions as

$$i\Gamma_{L/R} = \Sigma^r_{L/R} - \Sigma^a_{L/R} = 2i\,\mathrm{Im}(\Sigma^r_{L/R}). \tag{3.14}$$

Now we can solve $G^<$ also when the bias voltage is present as

$$\begin{aligned} G^<(\mathbf{r},\mathbf{r}';\omega) = \\ &- if_R(\omega)\int_{\partial\Omega_R}\int_{\partial\Omega_R} G^r(\mathbf{r},\mathbf{r}_R;\omega)\,\Gamma_R(\mathbf{r}_R,\mathbf{r}'_R;\omega)\,G^a(\mathbf{r}'_R,\mathbf{r}';\omega)\,d\mathbf{r}_R\,d\mathbf{r}'_R \\ &- if_L(\omega)\int_{\partial\Omega_L}\int_{\partial\Omega_L} G^r(\mathbf{r},\mathbf{r}_L;\omega)\,\Gamma_L(\mathbf{r}_L,\mathbf{r}'_L;\omega)\,G^a(\mathbf{r}'_L,\mathbf{r}';\omega)\,d\mathbf{r}_L\,d\mathbf{r}'_L. \end{aligned} \tag{3.15}$$

Note that bias voltage defines the difference between f_R and f_L. The electron density is calculated from $G^<$ as

$$\rho(\mathbf{r}) = \frac{-1}{2\pi}\int_{-\infty}^{\infty}\mathrm{Im}[G^<(\mathbf{r},\mathbf{r};\omega)]d\omega. \tag{3.16}$$

When we know the electron density we next calculate the new effective potential for the self-consistent iteration, and continue the iterations until the density or the potential do not change anymore.

After the self-consistent calculations, we know the effective potential, and calculate the electric current through the nanostructure. In order to do that we need to calculate the electron tunneling probability between the two leads. It is obtained from the function values at the boundaries $\partial\Omega_{L/R}$ as

$$\begin{aligned} T(\omega) = \int_{\partial\Omega_L}\int_{\partial\Omega_L}\int_{\partial\Omega_R}\int_{\partial\Omega_R} &\Gamma_L(\mathbf{r}_L,\mathbf{r}'_L;\omega)G^r(\mathbf{r}'_L,\mathbf{r}_R;\omega) \\ &\times\Gamma_R(\mathbf{r}_R,\mathbf{r}'_R;\omega)G^a(\mathbf{r}'_R,\mathbf{r}_L;\omega)\,d\mathbf{r}_L\,d\mathbf{r}'_L\,d\mathbf{r}_R\,d\mathbf{r}'_R. \end{aligned} \tag{3.17}$$

The current is then calculated as

$$I = \frac{1}{\pi}\int_{-\infty}^{\infty} T(\omega)\,(f_L(\omega) - f_R(\omega))\,d\omega. \tag{3.18}$$

Note that the tunneling probability is not the real probability in the sense that it can be larger than one. It includes the summation over the different conducting channels where one channel causes the conductance of one conductance quantum. Information about the local density of states in the leads is included in the $\Gamma_{L/R}$-functions.

3.3 Pseudopotentials

A typical three-dimensional nano-transport system is composed of a group of atoms. In a usual problem the positions of the nuclei are given and the task is to calculate the electron density. The core electrons are strongly localized near the nuclei, causing the electron density to change rapidly in the ion cores. The core electrons do not participate in forming the chemical bonds but this important phenomenon is due to the delocalized valence electrons. However, the core electrons cause, due to the orthogonality requirement, the valence electron wave functions to oscillate rapidly in the ion cores. Because the fast oscillations require a lot effort in numerical calculations it is practical to replace the ions with the pseudopotential operators.

In the pseudopotential formalism we write the single-particle wave function for the valence electrons $\Psi_v(\mathbf{r})$ in the from

$$\Psi_v(\mathbf{r}) = \phi_v(\mathbf{r}) + \sum_c \alpha_{cv}\Psi_c(\mathbf{r}), \tag{3.19}$$

where $\Psi_c(\mathbf{r})$ is a core electron wave function and ϕ_v a smoothly behaving function. The second term on the right hand side takes care of the orthogonalization of the Ψ_v regards Ψ_c. The coefficients α_{cv} can be calculated by multiplying both sides of the equation by $\Psi_c(\mathbf{r})$ and integrating over the space

$$\alpha_{cv} = -\int \phi_v(\mathbf{r}')\,\Psi_c(\mathbf{r}')\,d\mathbf{r}'. \tag{3.20}$$

Because $\Psi_v(\mathbf{r})$ is also an eigenfunction of the Hamiltonian $\hat{H}$ with eigenenergy ω_v we can write

$$\hat{H}\phi_v(\mathbf{r}) + \sum_c \int (\omega_v - \omega_c)\,\Psi_c(\mathbf{r}')\,\phi_v(\mathbf{r}')\,d\mathbf{r}'\,\Psi_c(\mathbf{r}) = \omega_v\phi_v(\mathbf{r}). \tag{3.21}$$

In this form we see that the new function ϕ_v is the solution of the eigenvalue equation which has the same eigenvalues as the original equation. Outside the atom core region $\phi_v(\mathbf{r})$ is equal to $\Psi_v(\mathbf{r})$. In this way we do not need to calculate the core electron states because their effects are included in the pseudopotential operator

$$\left(\hat{V}_{\mathrm{pse}}\,\phi_v\right)(\mathbf{r}) = \sum_c \int (\omega_v - \omega_c)\,\Psi_c(\mathbf{r}')\,\phi_v(\mathbf{r}')\,d\mathbf{r}'\,\Psi_c(\mathbf{r}). \tag{3.22}$$

In practice, besides of getting rid of the core electron states we also want our wavefunction to behave as smoothly as possible, so that the numerical problem is

easy to solve. This is why the pseudopotential operator is replaced with an operator which gives the same ϕ_v as the original one outside the core region (there $\phi_v \approx \Phi_v$), but makes ϕ_v smooth inside the core region. The pseudopotentials should have the same scattering properties as the original atoms. In this way the choice of the pseudopotentials is not unique and different types of pseudopotentials are suitable for different problems. Even if there are some problems concerning the use of pseudopotentials, the saving of computational time makes them very useful.

The use of pseudopotentials in the Green's function formalism is straightforward. The Green's functions are calculated using the Hamiltonian

$$\hat{H}(\mathbf{r}) = -\frac{1}{2}\nabla^2 + V_{\mathrm{ext}}(\mathbf{r}) + V_{\mathrm{c}}(\mathbf{r}) + V_{\mathrm{xc}}(\mathbf{r}) + \hat{V}_{\mathrm{pse}}(\mathbf{r}), \tag{3.23}$$

where $\hat{V}_{\mathrm{pse}}(\mathbf{r})$ is a non-local pseudopotential operator (see equation (3.22)) which is non-zero only for distances less than r_c from the ions cores. r_c is the so-called cut off distance, which depends on the type of the pseudopotential and the type of the atom.

In this work we use the norm-conserving non-local pseudopotentials generated with the FHI pseudopotential package [35, 36].

3.4 k-point sampling

Atomic layer structures can be modeled in the simplest form using models invariant in the transverse directions and therefore they are computationally one-dimensional. This we have done in Publication **IV** in the case of a magnetic resonant tunneling diode. However if the full atomistic structure is included three-dimensional models have to be used. The system is infinite not only in the transport direction but also in the perpendicular directions. The periodic boundary conditions with the **k**-point sampling [7] is the way how the widening of the system is implemented.

The idea behind the **k**-points is demonstrated in Figure 3.1 using a simple one-dimensional model. The wave functions and in our case the Green's functions are waves whose wavelength depend on the electron energy. In an infinite system the electron energy is a continuous variable. Now in order to make the simulation we cut from the system a small piece which is repeated periodically and fills the whole infinite system. When the periodic boundary conditions are applied (Figure 3.1) the electrons obtain an artificial discrete energy spectrum. In order to reduce the effect of this discreteness Green's functions are calculated using the

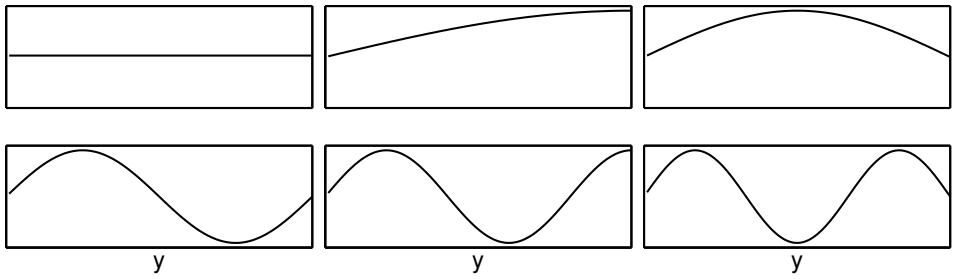

(a) $\phi = 0$ (b) $\phi = \frac{1}{2}\pi$ (c) $\phi = \pi$

Figure 3.1: One-dimensional demonstration of the meaning of **k**-points. The two lowest electron wave function states corresponding to different **k**-points are shown.

boundary conditions where a wave has a phase shift on the boundary. As a result we get a continuous energy spectrum which depends on the phase shift, because the wavelength can be something else than a multiple of the width of the region. The phase shifts in different directions are typically visualized as a points in the ϕ_x,ϕ_z and ϕ_z coordinates. This is why they are called as **k**-points. In the electronic structure calculations the number of **k**-points is then increased until the convergence is reached.

The periodic boundary conditions have a strong effect on the tunneling probability profile [37] as demonstrated also in Figure 3.2 using a flat potential. The Green's functions now behave like in a one-dimensional wave guide as it is seen in the profile. Every perpendicular eigenvalue causes a distorted step to the profile. In order to get a good result the number of k-points has to be so large that the average of the curves is smooth as the true solution is.

It must be noted that the Green's function $G^r(\mathbf{r}, \mathbf{r}')$ is symmetric and so is the numerical coefficient matrix. However, when **k**-points are included the situation changes. This is seen when we consider G^r at two points on the opposite boundaries $G^r(\mathbf{r}_{P1}, \mathbf{r}')$ from $\partial\Omega_{P1}$ and $G^r(\mathbf{r}_{P2}, \mathbf{r}')$ from $\partial\Omega_{P2}$ (see Fig. 2.3). These point have the same x and y coordinates so that when the periodic boundary conditions are implemented they satisfy

$$G^r(x_{P1}, y_{P1}, z_{P1}, \mathbf{r}') = G^r(x_{P1}, y_{P1}, z_{P1} + A_z, \mathbf{r}') \tag{3.24}$$

where A_z is the width of the region Ω along the z-direction. When the **k**-point corresponding to the phase shift ϕ is applied the equations have the forms

$$\begin{aligned} G^r(x_{P1}, y_{P1}, z_{P1}, \mathbf{r}') &= e^{i\phi}\ G^r(x_{P1}, y_{P1}, z_{P1} + A_z, \mathbf{r}') \\ G^r(x_{P1}, y_{P1}, z_{P1} + A_z, \mathbf{r}') &= e^{-i\phi}\, G^r(x_{P1}, y_{P1}, z_{P1}, \mathbf{r}') \end{aligned} \tag{3.25}$$

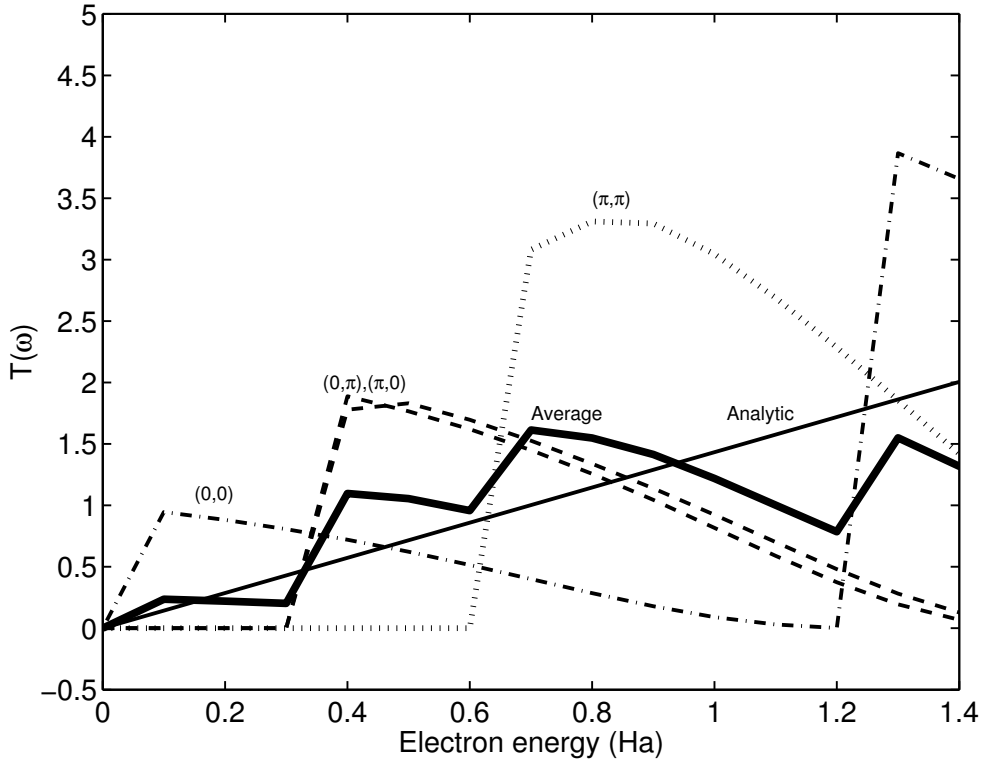

Figure 3.2: Effect of the number of **k**-points on the tunneling probability. The figure demonstrates the worst case in which the potential is totally flat. The calculation volume Ω is a cube with the size $3\,a_0 \times 3\,a_0 \times 3\,a_0$. The tunneling probability of different **k**-point channels are marked with broken and dotted lines. As is shown, one conducting channel produces a staircase tunneling profile. Using four k-points (ϕ= {(0,0),(0,π),(π,0)(π,π)}) the shape of the total tunneling curve (thick solid line) is still poor when compared to the analytic results (thin solid line).

The **k**-points giving real phase factors are ϕ = {(0,0), (0,π), (π,0), (π,π)}. They give symmetric and real boundary conditions, $\exp(i\phi)$={-1,1}. If other k-points are applied this is not true, and the Green's functions coefficient matrix is no more symmetric. The boundary conditions give a Hermitian component to the otherwise complex symmetric problem. This increases the memory and the computational time requirements of the simulations, because general complex routines have to be used.

Chapter 4

Numerical implementation

4.1 Finite element method

The numerical implementations of the Green's function solvers are done using the finite element method (FEM). This method is widely used in many different fields, for example, in structural mechanics, fluid dynamics, electromagnetics and heat transfer calculations. The FEM is a flexible method, because it allows different geometries and boundary conditions to be implemented in a straightforward way.

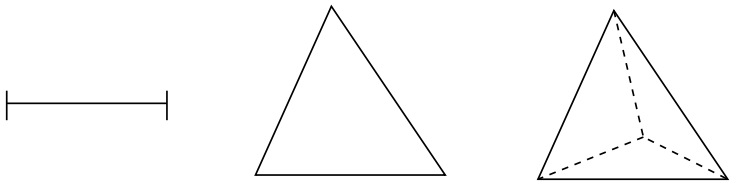

Figure 4.1: Shapes of different elements. In the two- and three-dimensional codes triangles and tetrahedra are used, respectively. Also quadrilateral, hexahedral and prismatic elements can be used.

In the FEM the calculation domain Ω is divided into small regions called elements. In this work we have used triangle elements in the two-dimensional solver and tetrahedra in the three-dimensional solver. These shapes have the advantage that their size can easily vary inside the domain region. The meshes of the elements are created using mesh generators. In this work we have used **Easymesh** [38] in the two-dimensional calculations and **Netgen** [39] in the three-dimensional ones. Both are so-called Delaunay-based generators [40].

The basis functions are constructed conforming to the mesh of the elements so that they are non-zero only in few neighboring elements. This ensures the local nature of the basis functions and the resulting matrices become sparse. Small elements imply many basis functions and so a good numerical accuracy can be achieved. This is how we can increase the accuracy in the regions where the solution changes fast. We have used the so-called *p*-elements which are introduced later in detail. They have a hierarchical high-order polynomial basis, which ensures a good convergence for smooth solutions.

4.2 Variational form of the equations

In order to use the FEM we have to first write the equations of the Green's function method in the variational form. $G^r(\mathbf{r},\mathbf{r}')$ is a solution of Equation (3.11) in the calculation volume which is introduced in Figure 2.3. Next we take a nicely-behaving arbitrary function $v(\mathbf{r})$ and multiply both sides of Equation (3.11) by it. Then we integrate over the calculation domain Ω. We use the properties of the open boundary system and make some manipulations [41] which are shown in detail in Publication **II**. After this the equation takes the form

$$\begin{aligned}\int_\Omega \Big\{ -\nabla v(\mathbf{r})\cdot\frac{1}{2}\nabla G^r(\mathbf{r},\mathbf{r}';\omega) + v(\mathbf{r})\big[\omega - V_{eff}(\mathbf{r})\big]G^r(\mathbf{r},\mathbf{r}';\omega)\Big\}\, d\mathbf{r} \\ - \langle\hat{\Sigma}_L G^r, v\rangle - \langle\hat{\Sigma}_R G^r, v\rangle = v(\mathbf{r}'),\end{aligned} \tag{4.1}$$

where the so-called self energy-operators have been derived to have the form

$$\begin{aligned}&\langle\hat{\Sigma}_{L/R} G^r, v\rangle = \\ &\int_{\partial\Omega_{L/R}}\int_{\partial\Omega_{L/R}} \frac{1}{4} G^r(\mathbf{r}'_{L/R},\mathbf{r}';\omega)\frac{\partial^2 g_e(\mathbf{r}_{L'/R'},\mathbf{r}_{L/R};\omega)}{\partial\mathbf{n}_{L/R}\partial\mathbf{n}_{L'/R'}}\, v(\mathbf{r}_{L/R})\, d\mathbf{r}_{L'/R'} d\mathbf{r}_{L/R}.\end{aligned} \tag{4.2}$$

The open boundary conditions of the system are included in the self-energy operators. They are the surface integrals over the open boundaries $\partial\Omega_{L/R}$. The function $g_e(\mathbf{r}_{L'/R'},\mathbf{r}_{L/R};\omega)$ is the Green's function of the isolated lead $\Omega_{L/R}$ with the zero boundary condition on the boundary $\partial\Omega_{L/R}$ [41]. In this equation $g_e(\mathbf{r}_{L'/R'},\mathbf{r}_{L/R};\omega)$ is differentiated with respect to both arguments in the direction of the normal vector $\mathbf{n}_{L/R}$ on the surface $\partial\Omega_{L/R}$.

Next we make the FEM approximation $G^r(\mathbf{r},\mathbf{r}';\omega) \approx G^r_h(\mathbf{r},\mathbf{r}';\omega)$. This means that we approximate the solution to be formed using a finite set of basis functions $S_h = [\phi_p \mid p = 1,2,\ldots,N]$ (see Equation (4.5) below). This basis does not cover

the whole functional space. In order to see the properties of the approximation we first shorten Equation (4.1) below to the form

$$a(G^r, v) = \langle \delta_{\mathbf{r}'}, v \rangle \ \forall v. \tag{4.3}$$

Above, a is a functional of G^r and v. $\langle\rangle$ marks inner product between functions. The FEM approximation fulfills Galerkin's orthogonality so that

$$\begin{aligned} a(G_h^r, v_h) &= \langle \delta_{\mathbf{r}'}, v_h \rangle \quad && \forall v_h \in S_h \\ \Rightarrow a(G_h^r - \delta_{\mathbf{r}'}, v_h) &= 0 && \forall v_h \in S_h \\ \Rightarrow a(G_h^r - G^r, v_h) &= 0 && \forall v_h \in S_h. \end{aligned} \tag{4.4}$$

This means that the approximation is a projection of the solution to the FEM basis and the discretation error is orthogonal to the approximation.

In the actual calculation the FEM approximation with the basis S_h is written in the form

$$G^r(\mathbf{r}, \mathbf{r}'; \omega) \approx G_n^r(\mathbf{r}, \mathbf{r}'; \omega) = \sum_{i,j=1}^{N} g_{ij}(\omega)\, \phi_i(\mathbf{r})\, \phi_j(\mathbf{r}'), \tag{4.5}$$

where $g_{ij}(\omega)$ are coefficients to be determined. We calculate t heir values for every electron energy ω by choosing

$$v(\mathbf{r}) = \phi_p(\mathbf{r}), \tag{4.6}$$

and inserting these in to Equation (4.1). The result is

$$\begin{aligned} g_{i,j}(\omega)\Big(\int_\Omega \Big\{ -\frac{1}{2}\nabla\phi_p(\mathbf{r}) \cdot \ \nabla\, \phi_i(\mathbf{r}) + \phi_p(\mathbf{r}) \big[\omega - V_{eff}(\mathbf{r})\big]\, \phi_i(\mathbf{r}) \Big\}\, d\mathbf{r} \\ - \langle \hat{\Sigma}_L\, \phi_i(\mathbf{r})\,, \phi_p \rangle - \langle \hat{\Sigma}_R\, \phi_i(\mathbf{r})\,, \phi_p \rangle \Big) \phi_j(\mathbf{r}') = \ \phi_p(\mathbf{r}'). \end{aligned} \tag{4.7}$$

Now the integrals can be performed and when j is chosen to be same as p we get a matrix equation which can be solved.

The solution includes a lot of integrals. In practice, these integrals are calculated using a reference element. This means that the points in an element in the mesh are mapped using an affine mapping to the reference element and the integrations are performed there using Gaussian quadrature rules. Integrals between the basis functions can be calculated and tabulated so that the constructions of the matrices are fast operations.

4.3 *P*-elements

There are some options how to choose a good finite-element basis [42]. The simplest choice is to use the linear elements so that the basis function is unity in one of the nodes and declines linearly to zero on the boundaries at the element. The linear basis is easiest to implement, but in order to achieve a better convergence high-order elements are used. For a smooth solution the difference in the accuracies between the linear and higher-order element calculations is huge. Because in our physical systems the solutions are typically relatively smooth we have implemented the so-called p-elements up to the fourth order.

The p-elements are hierarchical in the sense that the higher-order basis set includes also the lower-order basis sets [43]. A basis set has four types of functions, node-edge-, face-, and element-based functions. The node-based functions, which are linear, are nonzero only in the volume of the elements which have a common node. Similarly an edge based function is nonzero in the elements which have a common edge. The element-based functions have their support only inside one element. Table 4.1 demonstrates how many different types of basis functions there are inside a given element for a specific order polynomial.

Table 4.1: Number of different types of basis functions in different dimensions and for different order polynomials.

	1D	2D	3D
1 order	2 node	3 node	4 node
2 order	1 element	3 edge	6 edge
3 order	1 element	3 edge	6 edge
		1 element	4 edge
4 order	1 element	3 edge	6 edge
		2 element	8 face
			1 element
total	5	15	35

The basis function set of the p-elements is derived using the Legendre polynomials. This ensures that their derivatives are *a priori* orthogonal to each other to the maximum amount. The orthogonality makes the solutions numerically stable even when using polynomials of high order. Otherwise the stability of linear systems can be a problem. The one-dimensional basis functions in the reference element are shown in Figure 4.2.

Even if the derivatives of the basis functions are as orthogonal as possible, in practice the overlap between the basis functions is larger than that for just linear

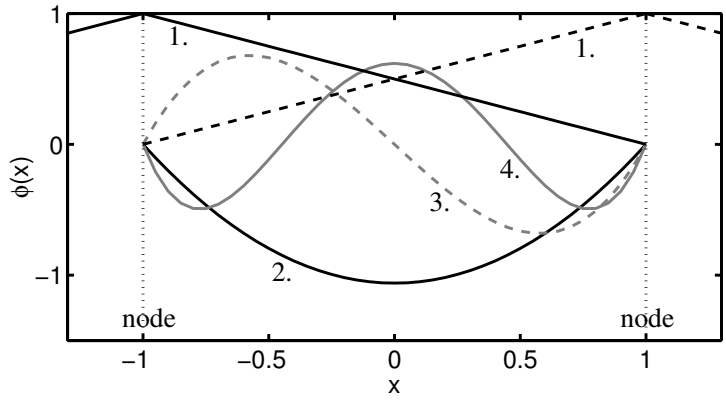

Figure 4.2: One-dimensional basis functions in the reference element [-1,1] up to the fourth order. Inside a element there are two node-functions and three element-functions (see Table 4.1)

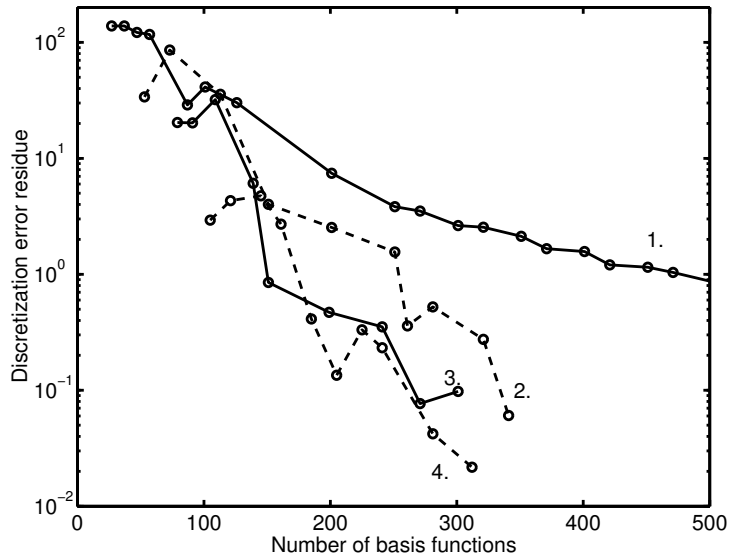

Figure 4.3: Discretization error as a function of the number of basis functions for different polynomial orders. The test case is a one-dimensional problem, the resonant tunneling diode (see Chapter 5.1). The error for the electron tunneling probability is calculated.

functions. Therefore when the number of the basis functions is reduced the filling of the coefficient matrix is increases. The filling of the matrices increases the CPU time and memory requirements when solving the equations. However, a smooth

solution converges faster for a larger filling. Therefore the critical factor for a good convergence with high-order polynomials is the smoothness of the solution. Figure 4.3 demonstrates in a one-dimensional case the convergence of the results as a function of the number of basis functions for different polynomial orders. Naturally, for each problem there is an optimal polynomial order.

4.4 Mixing schemes

In the DFT modeling the Kohn Sham equations are solved self-consistently for the electron density and the effective potential. In this work we combine these techniques with the Green's function methods. The problem cannot be solved directly as in the case of an explicit wave-function scheme [44], but we have to resort to iterative methods. This means that initially the electron density is calculated using a guessed effective potential, then a new potential is calculated from this electron density, and the electron density is calculated again. In order to obtain a convergent process the new effective potential cannot be used directly, but it has to be mixed with the old one. The simplest mixing scheme is the linear one

$$V_{\text{eff}}^{\text{in},i+1} = (1-\alpha)V_{\text{eff}}^{\text{in},i} + \alpha V_{\text{eff}}^{\text{out},i}, \tag{4.8}$$

where the potential $V_{\text{eff}}^{\text{in},i}$ is used to calculate the potential $V_{\text{eff}}^{\text{out},i}$. α is the mixing parameter which is typically $0.05 - 0.2$ in systems modeled in this work.

Even if the linear mixing scheme is simple it works quite reasonably. The benefit of it is simple programming and modest use of computer memory. Convergence is usually reached if α is small enough. This mixing scheme is used in our one- and two-dimensional calculations.

In our three-dimensional code, besides the linear mixing scheme another one, the so-called guaranteed-reduction-Pulay (GR-Pulay) mixing scheme, [45] is used. This scheme considers the L^2-residue of the effective potential, i.e.

$$\partial V_i = \sqrt{\int_\Omega \left[V_{\text{eff}}^{\text{in},i}(\mathbf{r}) - V_{\text{eff}}^{\text{out},i}(\mathbf{r})\right]^2 d\mathbf{r}}. \tag{4.9}$$

For a converged result the residue vanishes. In the GR-Pulay method a linear approximation is done using the potentials from the N previous iterations so that

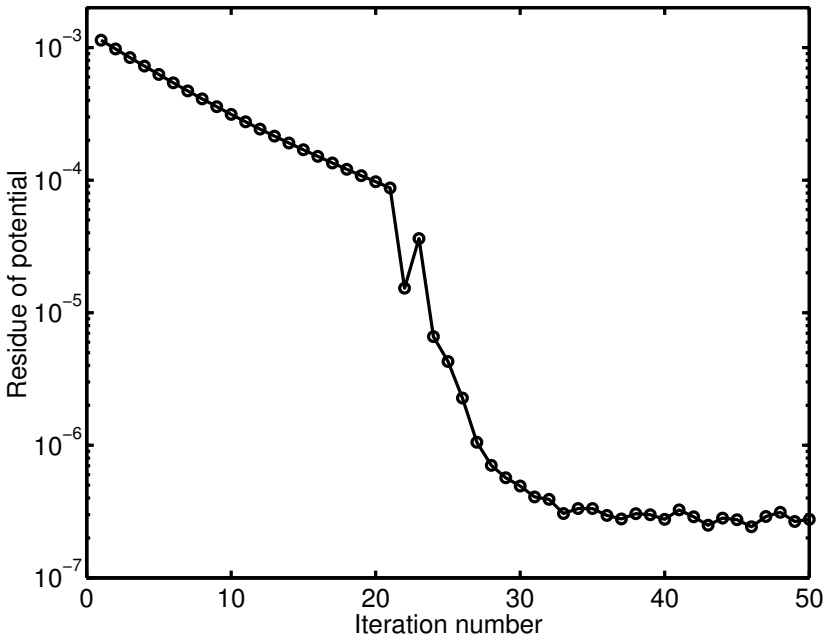

Figure 4.4: Residue of the potential V_{eff} as a function of the self-consistent iterations. The first 21 iterations are done using a linear mixing with a feed-back coefficient $\alpha = 0.15$. The rest of the iterations is done using the GR-Pulay method [45]. After 35 iterations the solution reaches the convergence. The remaining residue is due to discretization errors of the solution. The test system here is the bentzene-1,4-dithiolate molecule between two jellium cones.

V_{eff} is a linear combination of them. Thus,

$$\begin{aligned} V_{\text{eff}}^{i+1} &\approx \sum_{j=i-N}^{i} \kappa_j V_{\text{eff}}^{j}, \\ \sum_j \kappa_j &= 1. \end{aligned} \tag{4.10}$$

The residue is also approximated to be the linear combination using same coefficients κ_i as

$$\partial V^{i+1} \approx \sum_{j=i-N}^{i} \kappa_j \partial V^{j}. \tag{4.11}$$

Now, the idea is to choose the coefficients κ_i so that the residue ∂V^{i+1} is minimized. This is done using Lagrange multipliers.

In practice, the linear approximation for the residue does not work accurately enough so that ∂V^{i+1} could be used on right hand side of Equation (4.10). Therefore the residues $\partial V^j, (j = i - N...i)$ have to be calculated from Equation (4.9). If this is not done, the round-off errors accumulate and the calculation does not show any convergence. Because we still want to use the latest potential in our calculations we take one step further and use

$$V_{\text{eff}}^{\text{in},i+1} = \sum_{j=i-N}^{i} \kappa_j V_{\text{eff}}^j + \sum_{j=i-N}^{i} \kappa_j \partial V^j. \tag{4.12}$$

Note that the latest iteration potential V_{eff}^i is used only in the residue calculations because we do not know its residue.

The GR-Pulay method does not work if the approximation is too far from the solution. This is because the linear approximation is not valid at all. But reasonably close to the solution the convergence is much faster than that with the linear mixing scheme as is demonstrated in Figure 4.4.

4.5 Coulomb potential

The electronic Coulomb interaction, the Hartree potential

$$V_{\text{c}}(\mathbf{r}) = \int \frac{\rho(\mathbf{r}') - \rho_+(\mathbf{r}')}{|\mathbf{r} - \mathbf{r}'|} d\mathbf{r}' \tag{4.13}$$

is included in the effective potential. Above ρ_+ is the positive charge density caused by positive background charge. The calculation of $V_{\text{c}}(\mathbf{r})$ directly from (4.13) is computationally a heavy operation. Fortunately, we can solve V_{c} in computationally one- and three-dimensional systems by using the Poisson equation.

In the two-dimensional electron gas systems we want to use a two-dimensional element mesh and the three-dimensional Poisson equation cannot be solved on it. The two-dimensional Poisson equation gives the solution of a system which is translationally invariant along the perpendicular missing direction and gives a logarithmic behavior for V_{c} whereas the true three-dimensional behavior is r^{-1}.

In order to increase the stability of the self-consistency iterations, we use the modified Poisson equation [46]. We add an extra term on both sides of the Poisson equation, i.e.

$$\left(\nabla^2 - k_P^2\right) V_{\text{c}}^{i+1}(\mathbf{r}) = -4\pi[\rho_+(\mathbf{r}) - \rho^i(\mathbf{r})] - k_{\text{P}}^2 V_{\text{c}}^i(\mathbf{r}). \tag{4.14}$$

Here i marks the iteration number, so that on the left-hand side there is the new potential and on the right-hand side is the old one. Close to the converged result the new potential is close to old one, $V_{\mathrm{c}}^{i+1} \approx V_{\mathrm{c}}^{i}$, and the extra term disappears from the equation. The parameter k_{P} has a remarkable effect on the stability and the convergence rate of the calculations. This is because for a large k_{P} the local charge differences and not those far away from the given point affect strongly on the solution. In the terms of physics, the long-range Coulomb interaction becomes screened. In large systems, where the charge density varies strongly (charge sloshing), this is a useful property.

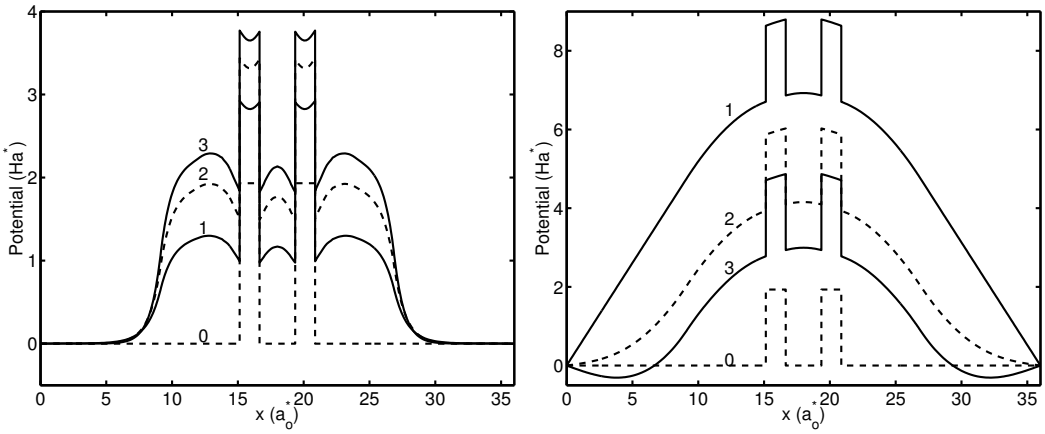

(a) $k_{\mathrm{P}} = 1$, $\alpha = 0.2$ (b) $k_{\mathrm{P}} = 0$, $\alpha = 0.01$

Figure 4.5: Effect of the different values of the k_{P} parameter to the iteration process of the effective potential. The test system is a resonant tunneling diode, for which the external potential has two potential barriers. Near the barriers there is no positive background charge. Close to the leads the charge density is constant. The effective potentials from the first iterations are shown for two sets of iteration parameters.

The effect of the k_{P} parameter is demonstrated in Figure. 4.5. For small values of the k_{P} parameter the potential sees the charge difference from a large volume and a small feedback parameter α is needed. Too large values of the k_{P} parameters cause the potential to connect too strongly to the old solution, slowing down the iteration rate. The final result does not depend on the choice of the k_{P} parameter.

In two-dimensional nanostructures the Poisson equation cannot be used and the original integral (4.13) has to be computed. Here the question is how to handle the point where $\mathbf{r} = \mathbf{r}'$ and the nominator vanishes [47]. Otherwise the integral is straightforward to evaluate. The problem is solved by using two changes of

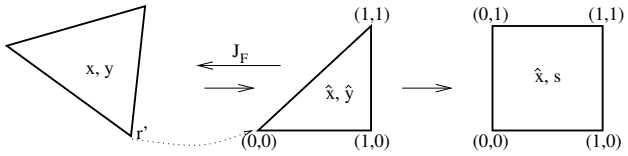

Figure 4.6: Coordinate transformations for the Coulomb integral calculation in two-dimensional electron gas systems.

variables. These changes are demonstrated in Figure 4.6. In the two-dimensional system we have triangular elements. We start from the situation, where $\mathbf{r}'$ is in one node of the triangle. An element where $\mathbf{r}'$ lies can always be divided into three smaller triangles so that $\mathbf{r}'$ is a node. We make the coordinate changes $(x, y) \rightarrow (\hat{x}, \hat{y})$ to an other element so that the $\mathbf{r}'$ mapped to the origin. This is given by an affine transformation

$$\begin{pmatrix} x \\ y \end{pmatrix} = J_F \begin{pmatrix} \hat{x} \\ \hat{y} \end{pmatrix} + \mathbf{b} = \begin{pmatrix} a_{11} & a_{12} \\ a_{21} & a_{22} \end{pmatrix} \begin{pmatrix} \hat{x} \\ \hat{y} \end{pmatrix} + \begin{pmatrix} b_1 \\ b_2 \end{pmatrix}. \tag{4.15}$$

After this we make another change $(\hat{x}, \hat{y}) \rightarrow (\hat{x}, s)$ so that $\hat{y} = s\hat{x}$. Using these changes we obtain

$$\begin{aligned} V_c(x', y') &= \int_T \frac{\rho(x, y) - \rho_+(x, y)}{\sqrt{(x - x')^2 + (y - y')^2}} \, dx \, dy \\ &= \int_0^1 \int_0^{\hat{x}} \frac{[\hat{\rho}(\hat{x}, \hat{y}) - \hat{\rho}_+(\hat{x}, \hat{y})] \, |\det J_F|}{\sqrt{(a_{11}\hat{x} + a_{12}\hat{y})^2 + (a_{21}\hat{x} + a_{22}\hat{y})^2}} \, d\hat{x} \, d\hat{y} \\ &= \int_0^1 \int_0^1 \frac{[\hat{\rho}(\hat{x}, s\hat{x}) - \hat{\rho}_+(\hat{x}, s\hat{x})] \, |\det J_F| \, \hat{x}}{\sqrt{(a_{11}\hat{x} + a_{12}s\hat{x})^2 + (a_{21}\hat{x} + a_{22}s\hat{x})^2}} \, dx \, ds \\ &= \int_0^1 \int_0^1 \frac{[\hat{\rho}(\hat{x}, s\hat{x}) - \hat{\rho}_+(\hat{x}, s\hat{x})] \, |\det J_F|}{\sqrt{(a_{11} + a_{12}s)^2 + (a_{21} + a_{22}s)^2}} \, dx \, ds. \end{aligned} \tag{4.16}$$

Note that now the pole has disappeared and the integral (4.16) does not have singularities. It can be evaluated by choosing the standard Gaussian quadrature rules for the both dimensions $\hat{x}$ and s.

4.6 Linear algebra

In the Green's function formalism most of the computational effort is going to the calculation of the electron density. Typically, in electronic structure simulations

single-particle electron wave functions and eigenvalues are explicitly solved. The eigenvalue problems are best to solve using iterative methods. However, in our method we need to solve linear equations. Typically several sets of equations have the same coefficient matrix and different right-hand sides, especially when matrices are inverted.

The best algorithm for solving linear equations with different right-hand sides and the same coefficient matrix is to use direct methods where the matrix is first factorized. Because our matrices are sparse we use direct sparse solvers which utilize the so-called multi-frontal method. The method is widely used in the solution of sparse linear systems [48, 49]. The actual implementation we use is in the Harwell Subroutine Library (HSL) [50] (see [51, 52] for other similar approaches).

4.7 Parallel implementation

As said above, most of the calculation time is spent in the calculation of the electron density. The calculation includes the numerical integration over the electron energy ω and it is easy to parallelize. Two- and three-dimensional versions of the Green's function solver are parallelized. In these version the integrals over the electron energy use a four-point Gaussian quadrature method. This is straightforward to parallelize by using two or four processors and the Message Passing Interface (MPI) library. This parallelization scales almost linearly with the number of processors.

After the above operations the parallelization can be improved by using two or more processors to calculate the same electron energy point. In our implementation this is also done using the MPI library. This means that all the processors have to make the factorization and save it to their own memory. This parallelization still works quite efficiently because most of the calculation time is spent in solving the equations and not on the factorization. However, it would be better to make this parallelization using shared-memory routines and the OpenMP library. This would solve the memory problems because then we could have more memory for a single factorization. During this work this was not possible, because there was not a proper shared-memory linear-equation library available.

Chapter 5

Results of nanostructure simulations

In this chapter we give a summary of our results for nanostructure simulations. In particular, we demonstrate that our solvers based on the density-functional theory and the non-equilibrium Green's function scheme can be used to simulate different types of nanostructures.

5.1 Magnetic resonant-tunneling diode

In addition to the non-equilibrium Green's function (GF) scheme, the Wigner function (WF) formalism is an alternative transport formalism. It includes semi-classical characteristics in contrast to the quantum-mechanical GF formalism. In Publication **III** we have compared these two formalisms by using a magnetic resonant tunneling diode as a test system. The calculations are done by using one-dimensional solvers.

The derivation [53, 54] of the WF formalism starts by making a coordinate transformation to the quantum mechanical density matrix

$$\rho(x, x') = \sum_i w_i \langle x|i\rangle\langle i|x'\rangle \,, \tag{5.1}$$

where x and x' are the one-dimensional spatial coordinates, $|i\rangle$ is a complete set of states, and w_i gives the probability of finding a particle in the state $|i\rangle$. The new coordinates, q and r, are given by the relations

$$\begin{aligned} q &= \frac{1}{2}(x + x') \\ r &= (x - x') \,. \end{aligned} \tag{5.2}$$

The WF $f(q,p)$ is now defined as the Fourier transform of the density matrix, i.e.

$$f(p,q) = \int_{-\infty}^{\infty} e^{-ipr} \rho(q + \frac{1}{2}r,\ q - \frac{1}{2}r) dr. \tag{5.3}$$

The result can be thought to be related to the classical phase-space representation. Because of the characteristic properties of quantum-mechanical systems f can, however, have even negative values. The WF formalism gives the same results as the GF formalism if the density matrixes $\rho(x,x')$ were calculated in the same way. However, the idea of the WF scheme is to use a lighter method, the quantum-mechanical Liouville–von Neumann equation

$$i\frac{\partial \rho}{\partial t} = [\hat{H}, \rho] \equiv \mathcal{L}\rho. \tag{5.4}$$

For this equation, totally open boundary conditions similar to the GF formalism do not exist. In our work we want to find out how well the WF formalism describes realistic systems in comparison with the GF scheme.

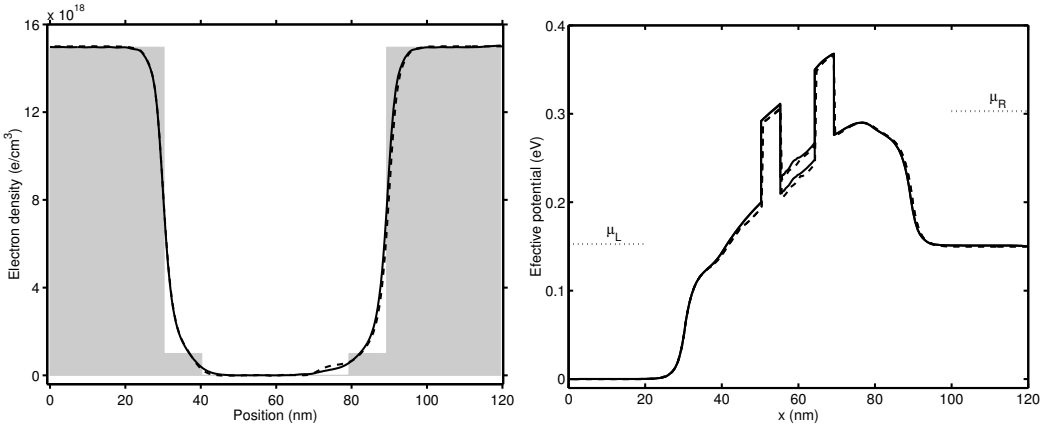

Figure 5.1: Simulation of a magnetic resonant tunneling diode consisting of a layer structure. The electron density and the effective potential for the resonance tunneling diode are given for the bias voltage of 0.15V. The shadowed areas denote the rigid positive background charge density, The solid and dashed curves denote the GF and WF solutions, respectively.

In order to make comparisons to the measurements we have chosen the parameters of our magnetic resonant-tunneling diode simulations similar to the actual diode made by Slobodskyy *et al.* [55]. Their diode works as a electron spin filter in an external magnetic field. We find that both the formalisms give similar results for the effective potential and the electron density as seen in Figure 5.1. In the

conductance there are, however, remarkable differences as seen in Figure 5.2. The active resonance peak, which is used to produce the spin polarized current, is the second one. The intensity of the first one is small. The WF has problems modeling this, because the method includes the Fourier transform for which the sharp changes are numerically difficult.

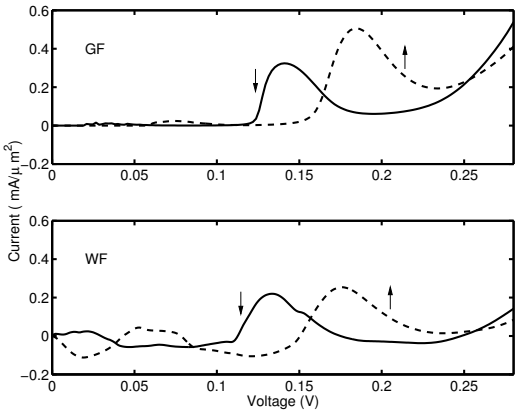

Figure 5.2: Simulation of a magnetic resonant tunneling diode consisting of a layer structure in the temperature of 4.3K and external magnetic field of 6T. Conductances of spin-up (↑) and spin-down (↓) electrons calculated using the GF and the WF formalism are given as a function of the bias voltage. The results correspond to a finite magnetic field splitting the spin degeneracy in the ZnMnSe layer between the potential barriers.

When the calculations are compared to the measurements, we find that the positions and the shapes of the resonance peaks are reasonable. Also the behaviors as a function of temperature and magnetic field show good agreement. The absolute value of the current is, however, about four orders of magnitude too large when compared to experiments. This is common with the results of other similar models and may be an artifact of the usage of the DFT, the ballistic transport model and the effective mass approximation.

5.2 Quantum wires

Two-dimensional nanostructures can fabricated at GaAs/AlGaAs interfaces as explained in Chapter 2. One of the simplest structures is a quantum wire. It is a thin nano-scale constriction between two bulk electrodes. If the wire is short compared to its width it is called as quantum point contact. We have modeled

quantum wires using the two-dimensional version our Green's function solver. The results are given in Publication **III** of the thesis.

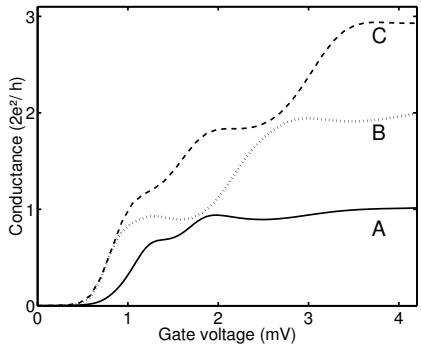

Figure 5.3: Conductance at zero temperature as a function of the gate voltage for three wires with the length L=7 a_0^* and widths S=5 a_0^* (A), 6 a_0 (B) and 10 a_0^* (C). The width of the electrodes is 20 a_0^*, and the length of the computational area is 47 a_0^*

Quantum wires are short so that electron transport through them is ballistic conserving the quantum-mechanical phase coherence. The conductance is quantized showing a staircase pattern with steps of the conductance quantum ($G_0 = 2e^2/h$) when measured as a function of the gate voltage [56, 57]. This is seen in Figure 5.3 for different widths of the quantum wire. In experiments the width can be controlled by another gate voltage. The quantum point contacts exhibit also the so-called 0.7-anomaly, which is a small plateau in the conductance around 0.7-0.5 G_0 [58, 59, 60].

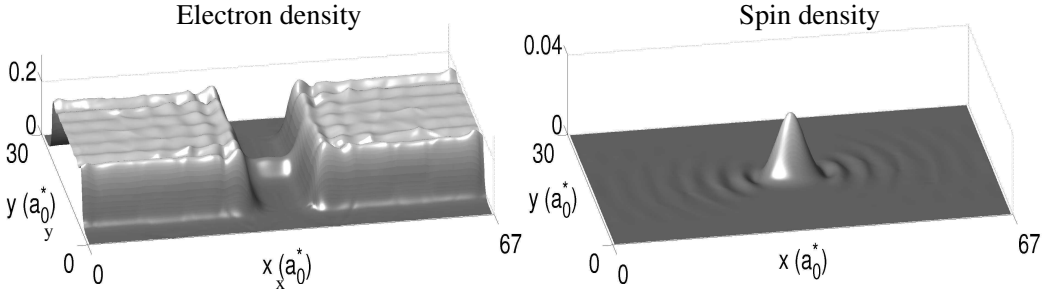

Figure 5.4: Total electron density and the difference between the spin-up and spin down electron densities at zero temperature for the quantum wire with the width of 5 a_0^*, and the length of 7 a_0^*. The positive background charge is reduced in the wire to describe the effect of a negative gate voltage above the wire.

Several models have been introduced to explain the 0,7-anomaly. Currently, the

many-body Kondo model based on the electron scattering off a dynamic spin appears as the most general one, explaining also the zero-bias anomaly observed [61, 62]. Our work and also other DFT calculations [62, 63] and recent experiments [64, 65] show indeed evidence localized magnetic moments in quantum point contacts.

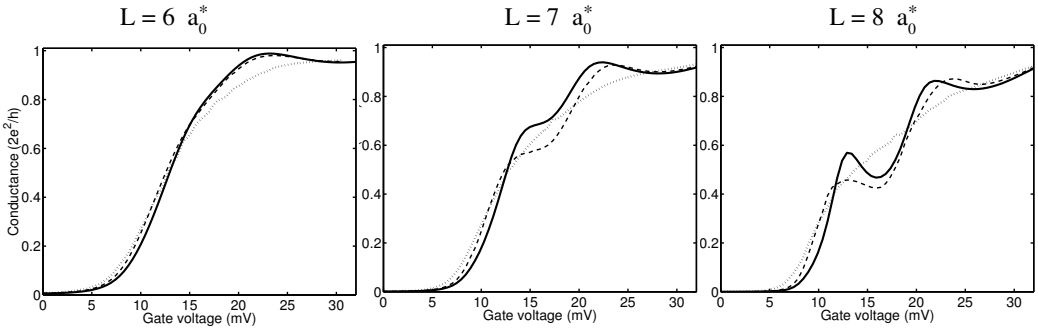

Figure 5.5: Conductance as a function of the gate voltage for quantum wires with the width of 5 a_0^* and lengths of 6 a_0^*, 7 a_0^* and 8 a_0^*. Temperatures are 0 K (solid curve), 2 K (dashed curve) and 4 K (dotted curve).

We make a simple model, in which the quantum wire and the leads are formed from a uniform positive background charge (see figure 5.4). This ensures the charge neutrality. In our model a spontaneous spin polarization causes the 0.7-anomaly. This is seen in Figure 5.5. The spin-polarization resulting in two peaks in the conductance is due to the spin-splitting of a resonance in the local density of states near the Fermi-level. It is also seen how the spin polarization increases as the temperature increases. This causes the descent of the plateau. The calculated current-gate-voltage curves as a function of the temperature and the wire length are similar to the measured ones.

5.3 Sodium nanowires

In Publication **I** we model atomic sodium wires. Lately we have used also the Green's function formalism in their modeling. The schemes used in these two calculations differ remarkably from each other even if the DFT is used in both of them. These results are a good example of problems the finite-size effects can cause in simulating nanostructures. The calculations in Publication **I** are done by using the cylindrically symmetric version of the MIKA code [1], and the Green's function solver calculations are performed by the three-dimensional code. Both of the codes employ non-local pseudopotentials for the Na atom chain.

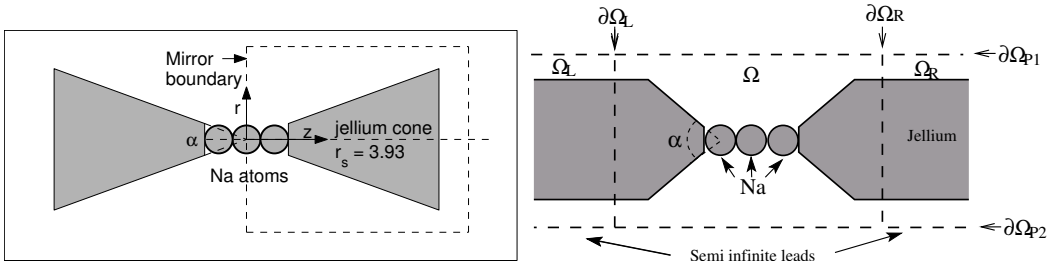

(a) Friedel-sum rule model

(b) Green's function model

Figure 5.6: Two models used in Na wire calculations. For the Friedel-sum model (a) have two finite size cones, whereas in the Green's function calculations (b) we connect the atom chain to semi-infinite leads.

The schematic picture of these models is shown in Figure 5.6. In the first model (Figure 5.6a) Na-atoms are located between two 'jellium' cones with the background charge density of sodium. The size of the cones is finite. Because the system has the mirror symmetry we can use the Friedel sum rule [66] for calculating the conductance. In the case of a sodium wire, there is only one conducting channel so that the rule results in a simple form for the conductance

$$G = G_0 \sin^2 \left[\frac{\pi}{2}(N_e - N_o) \right], \tag{5.5}$$

where N_e and N_0 are the numbers of electrons in the even and odd states, respectively. G_0 is the conductance quantum (Equation (2.5)). In zero temperature N_e and N_o are integers. However, in a finite temperature electron states are filled according of Fermi distribution and this means that some of the states are only partially filled. The use of this model is inspired the work by by Sim *et al.* [67]. They have used the same model with finite atomistic conical leads.

The model used in the Green's function calculations shown in Figure 5.6b is quite similar. Again Na atoms are between two cones, but now the cones are connected to semi-infinite leads. In order to make a good comparison the atomic distances and the cone geometry are chosen to be the same.

The results of these two models for conductance as a function of the number of Na-atoms in the wire are clearly different as seen Figure 5.7. Both models give even-odd oscillations as a function of the number of atoms in the wire. Our present interpretation is that the finite-size effects cause the result of Publication **I** the oscillations to change their phase when the cone angle is changed.

In the Green's function model calculations the conductance shows only small changes when the cone angle is changed and the phase of the oscillations does not

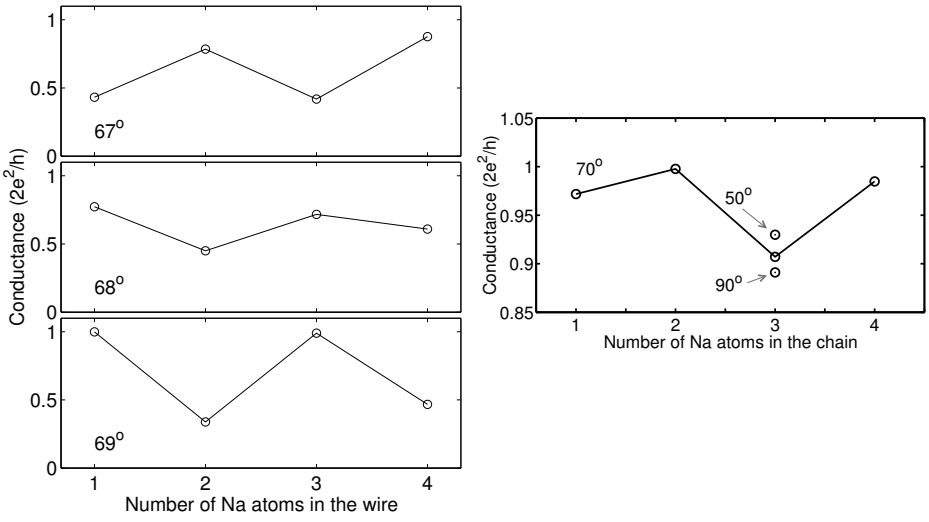

(a) Friedel sum model (b) Green's function model

Figure 5.7: Conductances of Na-atom wires as function of atoms in the wire. (a) Results of the Friedel-sum rule model and (b) those of the Green's function model are shown.

change remarkably. Figure 5.7b shows the results for the cone angle of 70°. The phase of the oscillation is in accord with Lang's calculations for Na atom chains between two semi-infinite jellium leads [68]. When we contact the Na atom chain to four Na atoms attached parallel to the jellium surface the phase of the oscillations changes so that the an even (odd) number of chain atoms corresponds to a minimum (maximum) conductance. This result is in accord with the Friedel sum rule calculations by Sim *et al.* [67] and the Green's function calculations by Lee *et al.* [69]. We note also that the amplitude of the conductance oscillations is consistently smaller in the Green's function calculations in comparison with the Friedel sum rule model.

5.4 Oxide layers

In MOSFET transistors the gate voltage is used to control the current between the source and the drain. The device is depicted in Figure 5.8. Between the gate electrode and the silicon region, where the current is flowing, there is a thin layer of insulating SiO_2. When the size of the transistors becomes smaller the question arises how thin a layer still works as insulator and further, can SiO_2 be

substituted by an insulator with better insulating properties. HfO_2 is seen as a good candidate for this purpose. This possibility is studied experimentally see, for example Ref. [70]

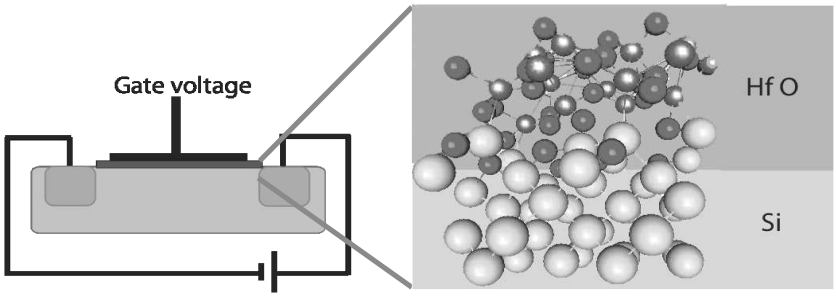

Figure 5.8: Structure of a MOSFET transistor. The drain and the source are made from strongly doped silicon. An insulating layer separates the metallic gate from the silicon part of the transistor. The gate voltage produces the conducting channel to the electrons or holes so that the current can flow from the drain to the source. Because the width of the conducting channel depends on the gate voltage, the gate voltage controls the size of the current.

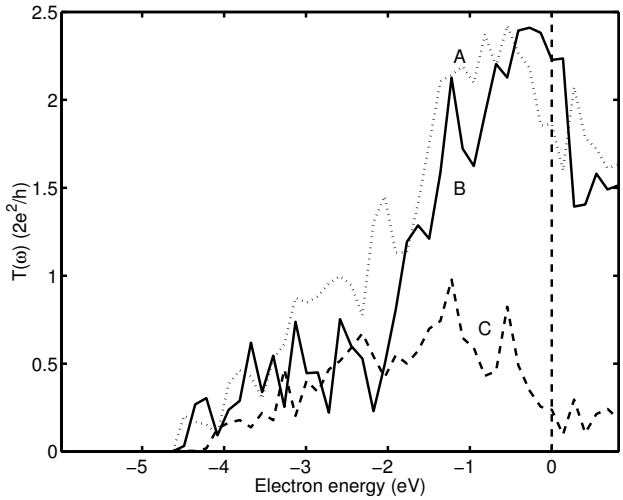

Figure 5.9: Tunneling probability trough HfO_2 -Si-layer structures as function of the electron energy. The structures A-C have different atomic arrangement near the interface.

Figure 5.9 gives our results for the tunneling probabilities through several different model structures consisting of Si and HfO_2 layers attached to two semi-infinite electrodes. The atomic coordinates are calculated using the SIESTA program [71]

which uses the DFT with an atomic orbital basis set. Model A is a stoichiometric and model B a non-stoichiometric interface. We find that during the atomic relaxation the oxygen atoms move from the HfO_2 to the silicon part. This causes silicon and hafnium to have metallic bonds and to form conducting channels through the interface and as is seen in Figure 5.9, the interface is not insulating. Model C is more ideal one. It is based on the calculation of Ref. [72]. There the atoms are placed close to the ideal lattice sites so that the result is insulating. The insulating properties are much better, although the tunneling probability is still finite at the Fermi-level.

Chapter 6

Summary

In this work we have modeled electronic and transport properties of nanostructures. In the modeling we have used the density-functional theory which is combined with Green's function methods. This means that instead of explicitly solving the single-particle wave functions, as it is typically done in the electronic structure calculations for materials, we have solved for single-particle Green's functions.

The Green's function method has many good features. For example, it is possible to implement so-called open boundary conditions. This means that electrons can travel through boundaries without any reflection or refraction making the finite-size effects small. The finite-size effects can be harmful in modeling open nanostructure systems, causing artificial results. Also, by using the Green's function method it is possible to calculate the electron tunneling probability and the current through the system for a finite bias voltage over the structure. An unfavorable feature of the Green's function-method is that the numerical calculations are heavier than those in typical wave-function methods.

In the present work we have implemented one-, two- and three-dimensional Green's function solvers using the finite element method. The finite element method is a flexible scheme. Different boundary conditions and shapes of the calculation domain are easy to define and implement. The local nature of the basis functions makes the coefficient matrix sparse. Also, varying the size of the finite-element mesh and the use of the higher-order polynomial basis reduce the need of the basis functions in comparison to the finite-difference method.

We have modeled different types of nanostructures. In Publication **IV** the Green's function formalism is compared to the Wigner function formalism by using a magnetic resonant tunneling diode as a test case. We find that both the formalisms give similar results. Numerically the Green's function method works better than the Wigner function method, because the latter uses Fourier transforms. Our sys-

tem exhibit sharp peaks in the density of states so that the transforms need many discretization points.

Quantum wires formed in the two-dimensional electron gas at semiconductor interfaces are modeled in Publication **III**. There we find in accordance with previous findings that the density-functional theory predicts a spontaneous spin polarization in the wire constriction. This causes the so-called 0.7-anomaly in the conductance as function of the gate voltage. The temperature behavior of the anomaly shows the correct trend. No traces of the zero-bias anomaly is seen indicating that this experimental finding is a more complicated many-particle effect.

Atomic Na chains are modeled in Publications **I** and **V**. In the former the Green's function formalism was not used, but instead the conductance is calculated using a wave function method and the Friedel-sum rule. We found that the conductance oscillates as a function of the number of atoms in the chain. The phase of the oscillations changes when the angles of the lead cones are varied. We have repeated these calculations later with the three-dimensional Green's functions solver. Now, when the finite-size effects are small, we see that the strong cone angle dependence has disappeared and the even-odd oscillation is much smaller. This is a good example of problems which can appear when using in the electron transport calculations wave functions restricted to a finite volume.

Thin HfO_2-Si interfaces were modeled in Publication **V**. There we find that the conductance properties depend strongly on detailed atomistic structures of the layers and interfaces. Oxygen atoms tend to move into silicon so that silicon and hafnium can have metallic bonds producing conducting channels through the interface. This reduces remarkably the insulating properties of the layers.

According to our work the density-functional theory combined with the Green's function formalism describes the coherent electron transport reasonably well in comparison with experiment. However, some problems are noticed. For example in some systems such as the one-dimensional resonant tunneling diode, the absolute value of the current is really too large, even if the shape of the curve is correct. The density-functional theory does neither describe all many-particle phenomena such as the Kondo effect. These phenomena can have a large effect on the transport properties. Apart from these limitations the density-functional theory combined with the Green's function scheme is a useful tool in the nanostructure modeling, because real structures of nanodevices can be included in the model. The systems can consist of actual atoms and not only of point-like atomic states.

Bibliography

[1] M. Heiskanen, T. Torsti, M. J. Puska, and R. M. Nieminen, *Multigrid method for electronic structure calculations*, Phys. Rev. B **63**, 245106 (2001).

[2] W. A. Hofer, A. S. Foster, and A. L. Shluger, *Theories of scanning probe microscopes at the atomic scale*, Rev. Mod. Phys. **75**, 1287 (2003).

[3] R. H. M. Smit, C. Untiedt, G. Rubio-Bollinger, R. C. Segers, and J. M. van Ruitenbeek, *Observation of a parity oscillation in the conductance of atomic wires*, Phys. Rev. Lett. **91**, 076805 (2003).

[4] S. Datta, *Electronic transport in mesoscopic systems* (Cambridge University Press, Cambridge, 1995).

[5] W. G. van der Wiel, S. D. Franceschi, J. M. Elzerman, T. Fujisawa, S. Tarucha, and L. P. Kouwenhoven, *Electron transport through double quantum dots*, Rev. Mod. Phys. **75**, 1 (2003).

[6] Y. Alhassid, *The statistical theory of quantum dots*, Rev. Mod. Phys. **72**, 895 (2000).

[7] N. W. Ashcroft and N. D. Mermin, *Solid State Physics* (Saunders College Publishing, USA, 1976).

[8] A. Nitzan, *Electron transmission through molecules and molecular interfaces*, Annu. Rev. Phys. Chem. **52**, 681 (2001).

[9] Cox and Zawadowski, *Exotic Kondo effects in metals: magnetic ions in a crystalline electric field and tunnelling centres*, Adv. in Phys. **47**, 599 (1998).

[10] G. D. Mahan, *Many-Particle Physics* (Kluwer Academic / Plenum Publishers, New York, 2000).

[11] J. Taylor, H. Guo, and J. Wang, *Ab initio modeling of quantum transport properties of molecular electronic devices*, Phys. Rev. B **63**, 245407 (2001).

[12] M. Brandbyge, J. Mozos, P. Ordejoń, J. L. Taylor, and K. Stokbro, *Density-functional method for nonequilibrium electron transport*, Phys. Rev. B **65**, 165401 (2002).

[13] M. B. Nardelli, J.-L. Fattebert, and J. Bernholc, *O(N) real-space method for ab initio quantum transport calculations: Application to carbon nanotube-metal contacts*, Phys. Rev. B **64**, 245423 (2001).

[14] P. S. Damle, A. W. Ghosh, and S. Datta, *Unified description of molecular conduction: From molecules to metallic wires*, Phys. Rev. B **64**, 201403(R) (2001).

[15] K. S. Thygesen, M. V. Bollinger, and K. W. Jacobsen, *Conductance calculations with a wavelet basis set*, Phys. Rev. B **67**, 115404 (2003).

[16] S.-H. Ke, H. U. Baranger, and W. Yang, *Electron transport through molecules: Self-consistent and non-self-consistent approaches*, Phys. Rev. B **70**, 085410 (2004).

[17] P. A. Khomyakov and G. Brocks, *Real-space finite-difference method for conductance calculations*, Phys. Rev. B **70**, 195402 (2004).

[18] E. Polizzi and A. N. Ben, *Subband decomposition approach for the simulation of quantum electron transport in nanostructures*, J. Comput. Phys. **202**, 150 (2005).

[19] P. Sautet and C. Joachim, *Electronic transmission coefficient for the single-impurity problem in the scattering-matrix approach*, Phys. Rev. B **38**, 12238 (1988).

[20] L. Chico, L. X. Benedict, S. G. Louie, and M. L. Cohen, *Quantum conductance of carbon nanotubes with defects*, Phys. Rev. B **54**, 2600 (1996).

[21] D. Wortmann, H. Ishida, and S. Bluegel, *An embedded Green-function approach to the ballistic electron transport through an interface*, Phys. Rev. B **66**, 075113 (2002).

[22] A. Calzolari, N. Marzari, I. Souza, and M. B. Nardelli, *Ab initio transport properties of nanostructures from maximally localized Wannier functions*, Phys. Rev. B **69**, 035108 (2004).

[23] P. Hohenberg and W. Kohn, *Inhomogeneous Electron Gas*, Phys. Rev. **136**, B864 (1964).

[24] W. Kohn and L. J. Sham, *Self-consistent equations including exchange and correlation effects*, Phys. Rev. **140**, A1133 (1965).

[25] W. Kohn., *Nobel Lecture: Electronic structure of matter, wave functions and density functionals*, Rev. Mod. Phys. **71**, 1253 (1999).

[26] R. O. Jones and O. Gunnarsson., *The density functional formalism, its applications and prospects*, Rev. Mod. Phys. **61**, 689 (1989).

[27] S. Lundqvist and N. H. March, *Theory of the inhomogeneous electron gas* (Plenum Press, New York, 1983).

[28] C. Attaccalite, S. Moroni, P. Gori-Giorgi, and G. B. Bachelet, *Correlation energy and spin polarization in the 2D electron gas*, Phys. Rev. Lett. **88**, 256601 (2002).

[29] P. Gori-Giorgi, C. Attaccalite, S. Moroni, and G. B. Bachelet, *Two-dimensional electron gas: correlation energy versus density and spin polarization*, Int. J. Quantum Chem. **91**, 126 (2003).

[30] D. M. Ceperley and B. J. Alder, *Ground state of the electron gas by a stochastic method*, Phys. Rev. Lett. **45**, 566 (1980).

[31] J. P. Perdew and A. Zunger, *Self-interaction correction to density-functional approximations for many-electron systems*, Phys. Rev. B **23**, 5048 (1981).

[32] G. Stefanucci and C.-O. Almbladh, *Time-dependent quantum transport: an exact formulation based on TDDFT*, Europhys. Lett. **67**, 14 (2004).

[33] G. Stefanucci and C.-O. Almbladh, *Time-dependent partition-free approach in resonant tunneling systems*, Phys. Rev. B **69**, 195318 (2004).

[34] Y. Xue, S. Datta, and M. A. Ratner, *First-principles based matrix Green's function approach to molecular electronic devices: general formalism*, Chem. Phys. **281**, 151 (2002).

[35] M. Fuchs and M. Scheffler, *Ab initio pseudopotentials for electronic structure calculations of poly-atomic systems using density-functional theory*, Comput. Phys. Commun. **119**, 67 (1999).

[36] N. Troullier and J. L. Martins, *Efficient pseudopotentials for plane-wave calculations*, Phys. Rev. B **43**, 1993 (1991).

[37] K. S. Thygesen and K. W. Jacobsen, *Interference and k-point sampling in the supercell approach to phase-coherent transport*, cond-mat/0411589 (2004).

[38] Two-dimension mesh generator Easymesh, see http://www-dinma.univ.trieste.it/nirftc/research/easymesh/Default.htm.

[39] Three-dimensional mesh generator Netgen, see http://www.hpfem.jku.at/netgen/index.html.

[40] M. Bern and D. Epstein, *Computing in Euclidean Geometry*, World Sci. Publishing, River Edge, NJ 23 (1992).

[41] T. J. R. Hughes, *Multiscale phenomena: Green's functions, the Dirichlet-to-Neumann formulation, subgrid models, bubbles and the origins of stabilized methods*, Comput. Methods Appl. Mech Engrg. **127**, 387 (1995).

[42] D. Braess, *Finite Elements* (Cambridge University Press, Cambridge, 1997).

[43] M. Ainsworth and J. Coyle, *Hierarchic finite element bases on unstructures tetrahedral meshes*, International Journal of Numerical Methods in Engineering **58**, 2103 (2003).

[44] M. C. Payne, M. P. Teter, D. C. Allan, T. A. Arias, and J. D. Joannopoulos, *Iterative minimization techniques for ab-initio total-energy calculations: molecular dynamics and conjugate gradients*, Rev. Mod. Phys. **64**, 1045 (1992).

[45] D. R. Bowler and M. J. Gillan, *An efficient and robust technique for achieving self consistency in electronic structure calculations*, Chem. Phys. Lett. **325**, 473 (2000).

[46] J. Arponen, P. Hautojärvi, R. Nieminen, and E. Pajanne, *Charge density and positron annihilation at lattice defects in aluminium*, J. Phys. F: Met. Phys. **3**, 2092 (1973).

[47] M. G. Duffy, *Quadrature over a pyramid or cube of integrands with singularity at a vertex*, SIAM Journal on Numerical Analysis **19**, 1260 (2003).

[48] J. K. Reid and I. S. Duff, *The multifrontal solution of indefinite sparse symmetric linear systems*, ACM Trans. on Math. Software **9**, 302 (1983).

[49] I. S. Duff, *A review of frontal methods for solving linear systems*, Computer Physics Communications **97**, 45 (1996).

[50] The Harwell Subroutine Library, see http://www.cse.clrc.ac.uk/nag/hsl/.

[51] A. Gupta, *WSMP: Watson Sparse Matrix Package Part II direct solution of general sparse systems*, IBM Research Report, RC **21886**, 98462 (2000).

[52] T. A. Davis, *A column pre-ordering strategy for the unsymmetric-pattern multifrontal method*, ACM Trans. Math. Software **30**, 353 (2004).

[53] W. R. Frensley, *Boundary conditions for open quantum systems driven far from equilibrium*, Rev. Mod. Phys. **62**, 745 (1990).

[54] C. Jacoboni and P. Bordone, *The Wigner-function approach to non-equilibrium electron transport*, Rep. Prog. Phys. **67**, 1033 (2004).

[55] A. Slobodskyy, C. Gould, T. Slobodskyy, C. R. Becker, G. Schmidt, and L. W. Molenkamp, *Voltage-Controlled Spin Selection in a Magnetic Resonant Tunneling Diode*, Phys. Rev. Lett. **90**, 246601 (2003).

[56] B. J. van Wees, H. van Houten, C. W. J. Beenakker, J. G. Williamson, L. P. Kouwenhoven, D. van der Marel, and C. T. Foxon, *Quantized conductance of point contacts in a two-dimensional electron gas*, Phys. Rev. Lett. **60**, 848 (1988).

[57] D. A. Wharam, T. J. Thornton, R. Newbury, M. Pepper, H. Ahmed, J. E. F. Frost, D. G. Hasko, D. C. Peacock, D. A. Ritchie, and G. A. C. Jones, *One-dimensional transport and the quantisation of the ballistic resistance*, J. Phys. C **21**, L209 (1988).

[58] B. E. Kane, G. R. Facer, A. S. Dzurak, N. E. Lumpkin, R. G. Clark, L. N. Pfeiffer, and K. W. West, *Quantized conductance in quantum wires with gate-controlled width and electron density*, Appl. Phys. Lett. **72**, 3506 (1998).

[59] K. J. Thomas, J. T. Nicholls, N. J. Appleyard, M. Y. Simmons, M. Pepper, D. R. Mace, W. R. Tribe, and D. A. Ritchie, *Interaction effects in a one-dimensional constriction*, Phys. Rev. B **58**, 4846 (1998).

[60] D. J. Reilly, T. M. Buehler, J. L. O'Brien, A. R. Hamilton, A. S. Dzurak, R. G. Clark, B. E. Kane, L. N. Pfeiffer, and K. W. West, *Density-Dependent spin polarization in ultra-low-disorder quantum wires*, Phys. Rev. Lett. **89**, 246801 (2002).

[61] Y. Meir, K. Hirose, and N. S. Wingreen, *Kondo model for the "0.7 anomaly" in transport through a quantum point contact*, Phys. Rev. Lett. **89**, 196802 (2002).

[62] K. Hirose, Y. Meir, and N. S. Wingreen, *Local moment formation in quantum point contacts*, Phys. Rev. Lett. **90**, 026804 (2003).

[63] K.-F. Berggren and I. I. Yakimenko, *Effects of exchange and electron correlation on conductance and nanomagnetism in ballistic semiconductor quantum point contacts*, Phys. Rev. B **66**, 085323 (2002).

[64] T. Morimoto, Y. Iwase, N. Aoki, T. Sasaki, Y. O. A. Shailos, J. P. Bird, M. P. Lilly, J. L. Reno, and J. A. Simmons, *Nonlocal resonant interaction between coupled quantum wires*, Appl. Phys. Lett. **82**, 3952 (2003).

[65] V. I. Puller, L. G. Mourokh, A. Shailos, and J. P. Bird, *Detection of local-moment formation using the resonant interaction between coupled quantum wires*, Phys. Rev. Lett. **92**, 096802 (2004).

[66] S. Datta and W. Tian, *Application of the Friedel sum rule to symmetric molecular conductors*, Phys. Rev. B **55**, R1914 (1997).

[67] H.-S. Sim, H.-W. Lee, and K. J. Chang, *Even-odd behavior of conductance in monatomic sodium wires*, Phys. Rev. Lett. **87**, 096803 (2001).

[68] N. D. Lang, *Anomalous dependence of resistance on length in atomic wires*, Phys. Rev. Lett. **79**, 1357 (1997).

[69] Y.-J. Lee, M. Brandbyge, M. J. Puska, J. Taylor, K. Stokbro, and R. M. Nieminen, *Electron transport through monovalent atomic wires*, Phys. Rev. B **69**, 125409 (2004).

[70] C. C. Hobbs *et al.*, *Fermi-level pinning at the polysilicon/metal oxide interface-Part I/II*, IEEE Transactions on Electron Devices **51**, 971 (2004).

[71] J. M. Soler, E. Artacho, J. D. Galea, A. García, J. Junquera, P. Ordejón, and D. Sánchez-Portal, *The Siesta method for ab initio order-N materials simulation*, J. Phys.: Condens. Matter **14**, 2745 (2002).

[72] L. R. Fonseca, A. A. Demkov, and A. Knizhnik, *Difficulties of the microscopic theory of leakage current through ultra-thin oxide barriers: point defects*, Phys. Stat. Sol. **239**, 48 (2003).